Graphene Quantum Dots as Nanoadditives in Cement Hydration: Mechanistic Insights into Pore Structure Refinement and Durability Enhancement

ACS OMEGA

Open Access

http://pubs.acs.org/journal/acsodf

Article

Graphene Quantum Dots as Nanoadditives in Cement Hydration: Mechanistic Insights into Pore Structure Refinement and Durability Enhancement

Thwe Thwe Win, Peem Nuaklong, Jintara Lawongkerd, Fahim Ullah, and Lapyote Prasittisopin*

Cite This: https://doi.org/10.1021/acsomega.6c03084

Read Online

ACCESS | Metrics & More | Article Recommendations

ABSTRACT: Graphene quantum dots (GQDs) have emerged as promising nanoscale modifiers for tailoring interfacial processes in cementitious systems; however, their mechanistic role in hydration and pore structure evolution remains insufficiently understood. The effects of dual-form GQDs (liquid and solid) on the structure−property relationships of concrete across multiple strength classes (24−42 MPa) were investigated. The results demonstrated that the incorporation of 0.1% liquid-form GQDs produced the most significant enhancement in concrete performance, achieving up to 32% improvement in 28-day compressive strength, 36% increase in splitting tensile strength, and approximately 18% increase in flexural strength compared with the control mixture. In addition, water absorption and porosity were reduced by approximately 25% and 32%, respectively, while acid resistance was significantly improved under aggressive exposure conditions. BET analysis further shows a substantial reduction (∼43%) in mesopore volume, confirming that GQDs govern pore structure evolution rather than acting solely as fillers. Notably, the dispersion state of GQDs critically influences performance, with liquid-phase GQDs exhibiting superior efficiency compared to their powdered counterparts due to improved interfacial distribution and reduced agglomeration. This study establishes a direct link between GQD-mediated cement chemistry, microstructural densification, and durability performance, providing a mechanistic framework for the design of next-generation nanoengineered cementitious materials for harsh service environments.

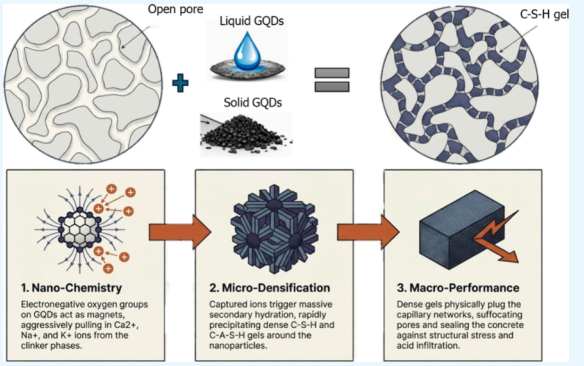

1. INTRODUCTION

The pursuit of improving concrete performance in harsh environmental conditions has led to the integration of diverse advanced materials, including nanoparticles, which exhibit distinctive mechanical, chemical, and electrical properties at the nanoscale.[1,2] The demand for concrete that satisfies strength criteria while exhibiting long-term durability is increasing, particularly due to the heightened exposure of concrete structures to severe conditions such as acid attacks, freeze−thaw cycles, and chloride ingress.[3−5] This has led researchers to investigate the use of nanoparticles to improve concrete performance, offering advantages in both strength and durability.[6]

Graphene, in its various forms, has shown considerable potential to improve the mechanical properties and durability of concrete.[7,8] Previous studies[9] reported that the effects of graphene nanoplatelets (GNPs) on the mechanical properties of cementitious composites. Similarly, Win et al.'s prior study on the integration of GNPs into calcium aluminate cement (CAC) systems showed that GNPs expedited CAC hydration and enhanced its resistance to acidic conditions.[8,10,11] In addition, Devi et al.[12] the recent studes[12,13] substantially advance the comprehension of graphene in building materials, especially in improving concrete performance. Their research on the influence of GO and reduced graphene oxide (rGO) on the mechanical properties of cementitious materials showed that these graphene derivatives significantly reduced the concrete matrix's porosity and facilitated the formation of more resilient hydration products.[14,15]

Durability is a vital consideration in the building sector. Concrete, a prevalent construction material, is susceptible to several degrading processes, including the infiltration of aggressive chemicals (e.g., CO_2, SO_4^{2-}, and Cl^-), alkali-silica reactions (ASR), calcium leaching, freeze−thaw cycles, and microbial attacks.[16] These concerns can considerably reduce its longevity. The development of more resilient materials is vital, but ongoing surveillance of civil infrastructure is equally

Received: March 20, 2026
Revised: June 24, 2026
Accepted: June 29, 2026

important for preserving structural integrity and prolonging its lifespan. Recent research has shown the beneficial effects of graphene-based nanosheets (GNS) on the durability of cementitious materials.[14] Nevertheless, existing research is limited, necessitating further studies to comprehensively elucidate the mechanisms by which GNS affects the long-term performance of concrete. The endurance of concrete in hostile conditions is essentially contingent upon its pore structure and permeability. Carbon nanotubes (CNTs) has been demonstrated improvements in durability by optimizing pore shape and altering transport characteristics within the cement matrix.[8,10,17] Experimental results demonstrate that these materials diminish water permeability, water sorptivity, and gas permeability, thereby enhancing resistance to hostile chemicals and prolonging the material's longevity.[18,19]

Unlike GO and GNPs, which primarily act as 2D mechanical reinforcements and nucleation sites but suffer from severe agglomeration at higher dosages,[20] Graphene quantum dots (GQDs) operate at the quantum scale[21,22] and achieve superior mesopore refinement without the agglomeration penalties typically seen in GO/GNP systems. These characteristics make GQDs an optimal choice for enhancing the mechanical, durability, and thermal properties of concrete.[23] Prior studies have shown that GQDs enhance the compressive and flexural strengths of mortar by refining the microstructure and promoting hydration in the early phases.[24,25] Shi et al.[22] investigated the effectiveness of GQDs in improving the performance of serpentine mortar under elevated temperatures. The incorporation of 0.03 wt % GQDs significantly enhanced compressive strength and reduced crystal water loss at 500 °C, indicating that GQDs can contribute to both mechanical improvement and thermal stability of cementitious composites.

Despite the promising performance of GQDs in cementitious materials, existing studies have primarily focused on mortar systems or single-strength concrete mixtures, with limited attention to durability under severe environments. Furthermore, the combined influence of GQDs on hydration behavior and pore structure evolution across multiple concrete strength classes remains insufficiently understood. The authors' previous studies mainly focused on the influence of graphene-based nanomaterials on hydration behavior, thermal performance, and mechanical enhancement of cementitious systems, including CAC composites.[8] However, the durability behavior of OPC concretes containing GQDs under acidic exposure conditions, particularly across multiple strength grades, remains insufficiently understood. Therefore, further investigation is necessary to establish a clearer structure−property−durability relationship governing GQDs-modified concrete systems.

Accordingly, this study presents a systematic investigation of dual-form GQDs in concretes with different strength classes (24, 28, 32, and 42 MPa) and at different doses (0.1% and 0.3% for liquid GQDs and 0.05% for solid GQDs, based on the weight of cement). The mechanical properties of concrete, including compressive, tensile, and flexural strengths, were assessed to evaluate its structural performance. After immersion in acidic solutions for 28 and 56 days, the durability traits, including water absorption, porosity, and acid resistance, were evaluated. To investigate the pore structure and chemical composition of concrete incorporating GQDs, the Brunauer−Emmett−Teller (BET) isotherm analysis and the thermogravimetric analysis (TGA) were conducted. X-ray diffraction (XRD) and field-emission scanning electron microscopy (FESEM), along with energy-dispersive spectroscopy (EDS), were also used to examine the concrete's phase composition and microstructure. This research aims to elucidate the potential of GQDs to ameliorate concrete performance, focusing on both mechanical strength and resistance to environmental deterioration. This study's findings enhance the existing knowledge on the use of GQDs in concrete, providing insights into the future of sustainable and high-performance building materials.

2. MATERIALS AND EXPERIMENTAL PROCEDURES

2.1. Materials

Ordinary Portland Cement (OPC) that meets ASTM C150[26] standard was used in this study. It had a specific gravity of 3.14 and a Blaine surface area of 3902 cm^2/g. The chemical composition of OPC was determined by X-ray fluorescence (XRF) analysis using a Bruker S8 Tiger instrument. The fine aggregate used was high-quality natural sand, complying with ASTM C33.[27] It had a specific gravity of 2.67, a fineness modulus of 2.91, and a water absorption rate of 0.63%. The particle size distribution of the fine aggregate is shown in Figure 1. The

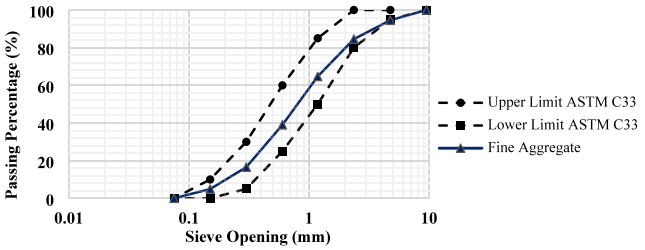

Figure 1. Sieve analysis of fine aggregate.

coarse aggregate used had a maximum particle size of 20 mm and a specific gravity of 2.66. To enhance the workability of the fresh mixtures, a modified polycarboxylate-based superplasticizer was incorporated. Manufactured by Sika, Thailand, this chloride-free admixture appeared as a light brown liquid, with a pH range of 4.5−6 and a density of 1060 kg/m^3. Tables 1 and 2 summarize the key

Table 1. Chemical and Physical Characteristics of OPC

OPC	weight %
SiO_2	18.70
Al_2O_3	5.38
Fe_2O_3	2.98
CaO	65.13
MgO	0.86
SO_3	4.21
Na_2O	0.42
K_2O	0.35
LOI	1.97
Blaine surface area (cm^2/g)	3862
specific gravity	3.15

Table 2. Properties of GQDs-L and GQDs-P

	values	
properties	GQDs-L	GQDs-P
electrical conductivity (S/m)		1.55
carbon content (%)		63.62
water content (wt.%)		12.21
apparent density (g/mL)	1.07	2.87
specific surface area (m^2/g)		189
particle size distribution (μm)		22.82

https://doi.org/10.1021/acsomega.6c03084
ACS Omega XXXX, XXX, XXX−XXX

characteristics of the raw materials used in the experiments. The study also investigated two types of GQDs synthesized. "GQDs-L," the first type, was in liquid form, while "GQDs-P," the second type, was a fine powder that included a suprastructure of GQDs-L assemblies. Both GQDs variants were obtained from CrystalLyte Company, Bangkok, Thailand. Figure 2 shows different-shaped GQDs that were made, and

Figure 2. GQDs-L (left) and GQDs-P (right) form.

Figure 3 shows the characterization results of GQDs that was studied with SEM-EDX, TEM, fluorescent property, Raman, and X-ray diffraction that was obtained from our previous study.[24,25]

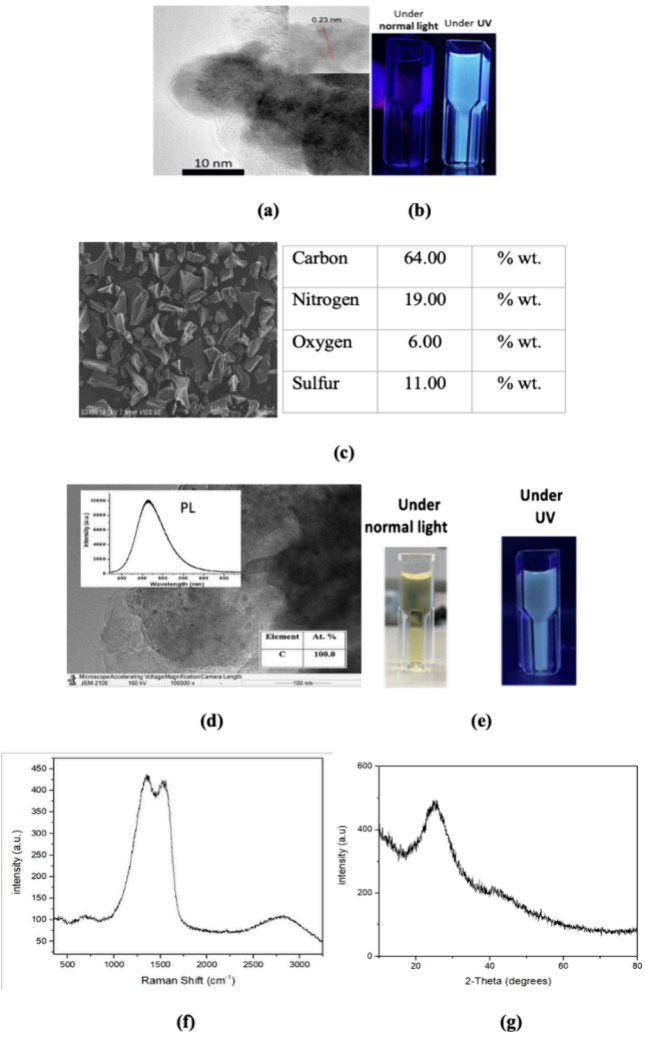

Figure 3. Characterization results of GQDs-L: (a) TEM and (b) fluorescent property, and characterization results of GQDs-P: (c) SEM-EDX, (d) TEM, (e) fluorescent property, (f) Raman, and (g) XRD.

2.2. Synthesis Method for GQDs

GQDs were synthesized via electrochemical reduction in a CO_2-saturated monoethanolamine (MEA) solution. The reaction was carried out in a custom-built reactor (approximately 12 × 17 × 16 cm) containing around 2 L of CO_2-MEA solution. Silver-coated copper foils and platinum foils were used as cathode and anode materials, respectively. The system operated under ambient conditions at a constant potential of −2.6 V for 12 min per cycle, repeated for 10 cycles, with the cathode replaced after each run [Patent No. WO2022185098A1].[28] The resulting colloidal solution was then vacuum-dried, dialyzed, and freeze-dried to isolate the GQDs. The product from the initial cycle was further treated by thermal drying at approximately 270 °C to remove unwanted byproducts. This material was then carbonized in a N_2 atmosphere at 600 °C for 1 h, with a controlled heating rate of 1 °C/min and a gas flow rate of 1000 mL/min. The obtained carbonized GQDs were finely ground and sieved through a 20−45 mesh screen to achieve a uniform powder as a nanoparticle additive.

2.3. Mixture Proportions

The mix proportions are provided in Table 3. The 16 mixture ratios incorporate varying amounts of liquid GQDs (0%, 0.1%, and 0.3%) and powder GQDs (0.05%), as additives to the concrete by weight of cement. Due to the relatively low dosage of GQDs-L compared with the total mixing water content, the additional liquid introduced through the suspension was considered negligible and did not significantly affect the effective water-to-cement ratio of the mixtures. The selected GQDs dosages are based on preliminary optimization and previous studies conducted by[24,25] on graphene-based nanomaterials in cementitious systems, where low dosages showed effective enhancement of hydration and mechanical performance while minimizing agglomeration effects. The control mix, designated GQDs0, was specifically formulated for concrete, ensuring compressive strengths of 24, 28, 32, and 42 MPa. A label clearly identified each mixture, indicating the content of GQDs-L and GQDs-P. For example, mix GQDs-L0.1 contained 0.1% GQDs-L, while mix GQDs-P0.05 contained 0.05% GQDs-P. The mixtures were carefully created in a controlled laboratory environment for thorough experimental examination. In this study, the total volume of water in the material matrix was kept constant. Hence, as the volume of cement increased, the water-to-cement ratio (w/c) decreased accordingly. A pan mixer was used to mix concrete. Fine aggregates and coarse aggregates were mixed for 3 min in the mixer. Cement was then added to the pan, and mixing was carried out for 2 min. In the control mix, two-thirds of the water was added first. A thorough mixing was then carried out for 2 min. Then, along with one-third of the water, the superplasticizer was added, followed by a 2 min mixing. For concrete with GQDs, water was added in 3 stages. The first one-third of water was added to the mix. After mixing the contents in the pan for 2 min, one-third of the water was added, followed by the superplasticizer. GQDs were added to the pan with the remaining water to ensure uniformity. Figure 4 presents the experimental program followed in this study.

2.4. Experimental Investigations

The tests of fresh and hardened properties of concrete are presented in this section. A slump test was conducted to determine the workability of the fresh concrete mixtures containing GQDs. Three specimens were tested for each experiment. The compressive strength of the mixes cured for 3, 7, and 28 days was determined using 150 mm cubes, as per BS EN 12390−3:2002.[29] Splitting tensile strength and flexural strength of concrete cured for 7 and 28 days were evaluated using cylinders (diameter 150 mm and height 300 mm) and prisms of dimensions 100 × 100 × 350 mm by adhering to BS EN 12390−6:2009[30] and BS EN 12390−5:2009[31] respectively. Again, three specimens were performed for each experiment. The durability assessment was limited to water absorption, porosity and acid attack resistance tests, which are essential for evaluating the long-term durability and performance of concrete. These tests are additional components in the durability assessment of concrete, according to ASTM C642.[32] Concrete cylinders with a diameter of 100 mm and a height of 100 mm were used for water

https://doi.org/10.1021/acsomega.6c03084
ACS Omega XXXX, XXX, XXX−XXX

Table 3. Mix Proportions of the Concrete

mix ID	mix design (MPa)	cement (kg/m^3)	water (kg/m^3)	fine aggregates (kg/m^3)	coarse aggregates (kg/m^3)	admixture (kg/m^3)	GQDs-L (kg/m^3)	GQDs-P (kg/m^3)	w/c	GQDs-L(%)	GDQs-P(%)	Slump (mm)
GQDs0	24	272	195	820	1150	1.09	0	0	0.72	0	0	140
GQDs-L0.1	24	272	195	820	1150	1.09	0.272	0	0.72	0.1	0	150
GQDs-L0.3	24	272	195	820	1150	1.09	0.816	0	0.72	0.3	0	160
GQDs-P0.05	24	272	195	820	1150	1.09	0	0.136	0.72	0	0.05	145
GQDs0	28	284	195	910	1040	1.14	0	0	0.69	0	0	135
GQDs-L0.1	28	284	195	910	1040	1.14	0.284	0	0.69	0.1	0	145
GQDs-L0.3	28	284	195	910	1040	1.14	0.852	0	0.69	0.3	0	150
GQDs-P0.05	28	284	195	910	1040	1.14	0	0.142	0.69	0	0.05	140
GQDs0	32	310	195	800	1140	1.24	0	0	0.63	0	0	130
GQDs-L0.1	32	310	195	800	1140	1.24	0.310	0	0.63	0.1	0	140
GQDs-L0.3	32	310	195	800	1140	1.24	0.930	0	0.63	0.3	0	145
GQDs-P0.05	32	310	195	800	1140	1.24	0	0.155	0.63	0	0.05	135
GQDs0	42	350	195	780	1120	1.40	0	0	0.56	0	0	125
GQDs-L0.1	42	350	195	780	1120	1.40	0.350	0	0.56	0.1	0	135
GQDs-L0.3	42	350	195	780	1120	1.40	1.050	0	0.56	0.3	0	140
GQDs-P0.05	42	350	195	780	1120	1.40	0	0.175	0.56	0	0.05	130

Figure 4. Schematic illustration of the experimental workflow.

absorption, porosity, and acid attack resistance tests after 28 days of water curing. The concrete specimens were immersed in a 50 g/L sulfuric acid (H_2SO_4) solution for 28 and 56 days at 23 °C. To maintain a stable acidic environment and consistent aggressiveness during the immersion period, the acid solution was periodically renewed every 7 days. In addition, the solution-to-specimen volume ratio was maintained at approximately 4:1 throughout the test. The change in their compressive strengths and mass loss after exposure to

https://doi.org/10.1021/acsomega.6c03084
ACS Omega XXXX, XXX, XXX−XXX

concentrated acid solution was evaluated. Once again, three specimens were tested for each experiment.

Microstructural analysis helps identify the causes of behavioral trends observed in tests conducted on hardened specimens. The BET isotherm is a promising method for assessing the adsorption properties of various materials. In this study, BET results were employed to characterize the pore properties of concrete, which are closely linked to its strength. This technique involved subjecting the sample to a vacuum, causing the cement matrix to adsorb nitrogen gas. A nitrogen adsorption measurement instrument (Micromeritics 3Flex, Micromeritics Instrument Corporation, USA) was used to quantify the amount of adsorbed N_2 gas, providing insights into different adsorption capacities. One g of the 28-day-cured sample was used for pore-structure analysis of concrete. The pore analysis covers sizes from 1 to 500 nm according to the BET theory. The results for concrete pore size and volume are reported accordingly. Additionally, the 28-day-cured powder samples were analyzed using a TGA instrument (PerkinElmer Pyris 1) to examine phase formation. The TGA experiment involved heating the samples from 25 to 1000 °C at a rate of 10 °C/min while maintaining a continuous flow of N_2 (70 mL/min). The central regions of the specimens were core-drilled to obtain powdered samples for further analysis. The BRUKER D8 DISCOVER instrument was used at 40 kV and 30 mA to do XRD. The Cu Kα radiation (λ = 0.154 nm) was used over a range of 5° to 80°, with a step size of 0.02° and a dwell time of 0.5 s per step. Additionally, comprehensive information regarding the crystalline phases of both unhydrated and hydrated products was extracted from established literature sources and the International Centre for Diffraction Data (ICDD) database, ensuring accurate phase identification. Moreover, the microstructural morphology of the concrete was examined using FESEM-EDS on a SUPRA 66VP SEM instrument (Oberkochen, Germany). The FESEM instrument was used to record and analyze the atomic-scale surface morphology of the specimens. To enhance electrical conductivity, the sample's fracture surface was coated with Au prior to testing. Subsequently, the coated samples were inserted into the FESEM machine, enabling image capture. The observed FESEM images commonly show the observed morphology. Figure 5 presents a flowchart illustrating the sequence of the experimental process followed in this study.

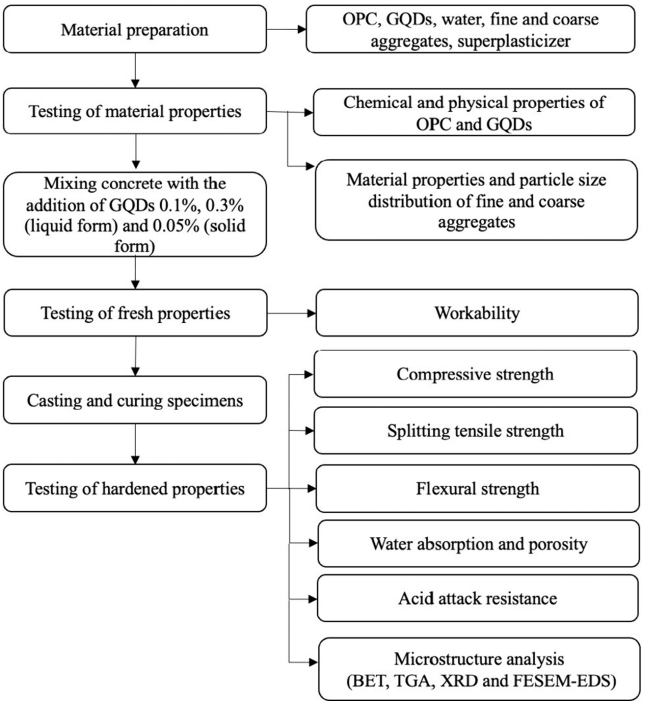

Figure 5. Flowchart illustrating the sequence of steps involved in the experimental program.

3. RESULTS AND DISCUSSIONS

3.1. Fresh Properties

It was found that the GQDs addition gradually increased the mix's fluidity during a conventional slump test. The measured

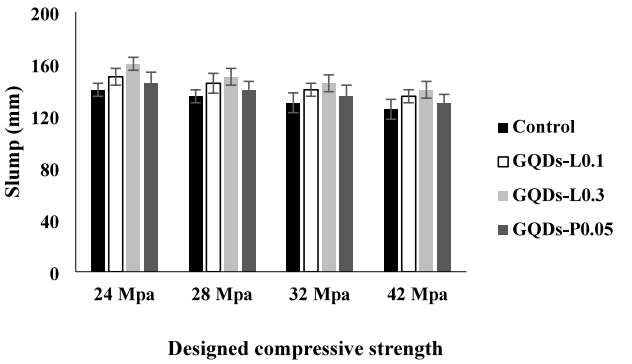

Figure 6. Slump for fresh concrete with GQDs.

slump values clearly show that increased GQDs dosages resulted in improved workability, as shown in Table 3 and Figure 6. This indicates that, compared with the control mix, GQDs directly and quantifiably improve the flowability and consistency of fresh concrete. Compared with the control mixes, the addition of GQDs continuously increased workability across all strength classes (24, 28, 32, and 42 MPa), with the effect being strongest at higher liquid GQDs concentrations. Concretes containing 0.3% liquid GQDs produced slumps as high as 160 mm in the 24 MPa class and 150 mm in the 28 MPa class, whereas the control mixes reported droop values in the range of 125 to 140 mm. Slump increased by 5 to 10 mm in all strength classes, even at smaller dosages (0.1% liquid form), although the powdered GQDs provided more subdued gains. This consistently rising slump with dosage suggests that GQDs actively alter the rheology of new mixtures. GQDs dissolve in the mixing water when added in liquid form, reducing agglomeration and guaranteeing even dispersion over the binder-aggregate matrix. This homogeneity improves the dispersing effectiveness of superplasticizers based on polycarboxylate ether (PCE), leading to increased cement particle separation and reduced inter-particle friction. As a result, the concrete is more fluid than the control.

The workability of GQDs is further improved by their hydrophilic properties. Water molecules are attracted to and retained by functional groups such as hydroxyl (−OH) and carboxyl (−COOH),[33] thereby increasing the amount of free water in the paste available for lubrication. This phenomenon indicates that, when GQDs are present, a more fluid mix is produced at the same w/c than when they are absent. This behavior is similar to how chemical admixtures reduce water content; surface interactions influence the amount of water available without changing the proportions of the combination as a whole.[34,35] It is interesting to note that the impacts were more noticeable in the concretes with lower and medium strengths (24 and 28 MPa) than in the higher-strength classes (32 and 42 MPa). This is because lower-strength mixes (lower cement contents) have a larger w/c, which intensifies the lubricating properties of GQDs. Since there is already less free water available in denser mixtures with lower w/c ratios, GQDs' relative contribution to workability is less noticeable. However, slump improved by up to 15 mm even in the 42 MPa class with

https://doi.org/10.1021/acsomega.6c03084
ACS Omega XXXX, XXX, XXX−XXX

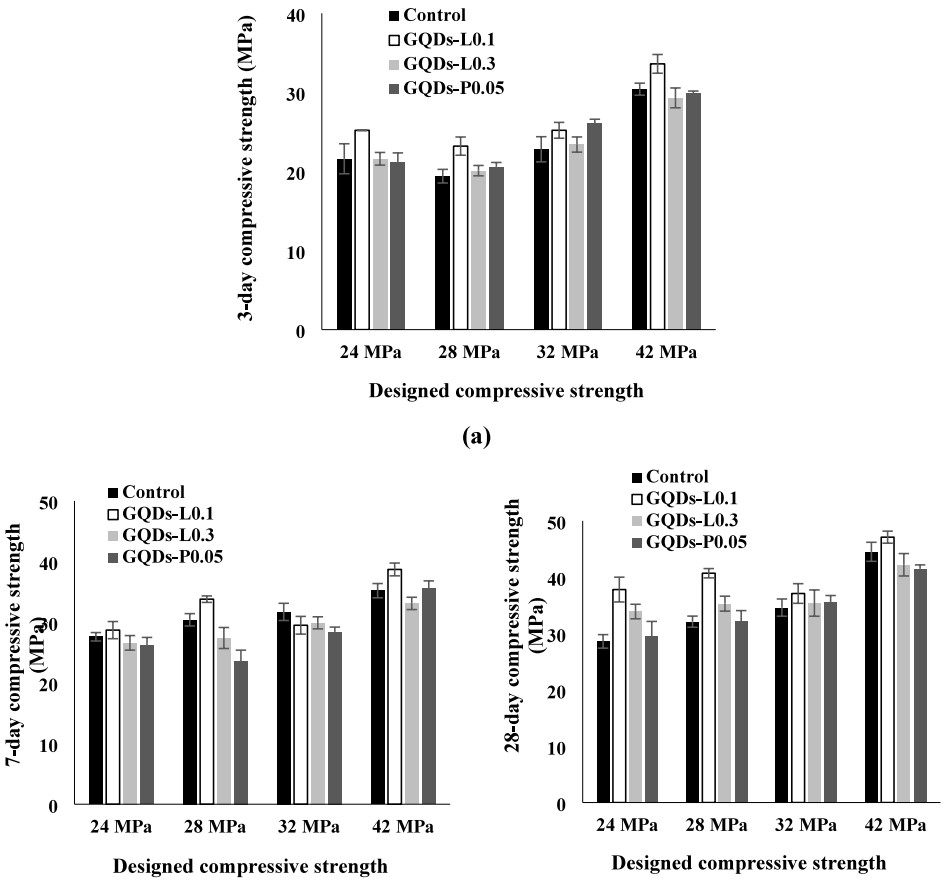

Figure 7. Compressive strength for concrete with GQDs: (a) 3-day strength, (b) 7-day strength, and (c) 28-day strength.

Table 4. Compressive Strength of Control and GQDs-Modified Concrete At 3, 7, and 28 Days[a]

strength class	age (days)	control (MPa)	GQDs-L0.1 (MPa)	GQDs-L0.3 (MPa)	GQDs-P0.05 (MPa)
24 MPa	3	21.6 ± 1.90	25.2 ± 0.05	21.6 ± 0.80	21.2 ± 1.14
	7	27.6 ± 0.70	28.7 ± 1.42	26.6 ± 1.20	26.2 ± 1.30
	28	28.6 ± 1.20	37.8 ± 2.20	33.9 ± 1.29	29.5 ± 2.64
28 MPa	3	19.4 ± 0.86	23.2 ± 1.15	20.1 ± 0.65	20.6 ± 0.53
	7	30.4 ± 1.02	33.8 ± 0.54	27.4 ± 1.73	23.6 ± 1.80
	28	32.1 ± 0.99	40.7 ± 0.83	35.3 ± 1.33	32.2 ± 1.87
32 MPa	3	22.8 ± 1.59	25.2 ± 1.00	23.4 ± 0.96	26.1 ± 0.50
	7	31.7 ± 1.42	29.5 ± 1.46	29.9 ± 1.00	28.4 ± 0.80
	28	34.6 ± 1.53	37.1 ± 1.75	35.4 ± 2.33	35.5 ± 1.24
42 MPa	3	30.4 ± 0.76	33.6 ± 1.18	29.3 ± 1.25	29.9 ± 0.26
	7	35.2 ± 1.18	38.7 ± 1.06	33.1 ± 1.02	35.6 ± 1.22
	28	44.5 ± 1.69	47.1 ± 1.07	42.2 ± 1.99	41.5 ± 0.68

[a]Data present the average value ± standard deviation.

0.3% liquid GQDs, demonstrating that the influence of GQDs is constant across mix designs, albeit to differing degrees.

Powdered GQDs were less successful because of the possibility of agglomeration and uneven dispersion, even if they produced slight improvements (usually +5 mm over the control). On the other hand, because liquid GQDs were easier to incorporate into the aqueous phase and interacted more smoothly with cement particles and admixtures, they consistently produced gains. Similar findings[36,37] showed that liquid-phase dispersions of graphene-based nanomaterials perform better than powdered versions in terms of preserving flowability and reducing clustering.

Previous research[24] supports this pattern, showing that correctly dosed graphene derivatives gradually enhance flowability. Researchers have used superplasticizers to improve the workability of cementitious composites containing GNPs.[38,39] The current findings demonstrate that GQDs offer a unique advantage in balancing workability and strength enhancement, especially when they are in liquid form. GQDs produce a more uniform cementitious matrix by enhancing dispersion and fluidity during the fresh stage, resulting in denser hydration products and better hardened properties.

3.2. Mechanical Properties

The results for the mechanical properties of the concrete, namely compressive strength, split tensile strength, and flexural strength, are presented in this section.

3.2.1. Compressive Strength. The results for curing ages (3, 7, and 28 days) and compressive strength for all strength classes (24, 28, 32, and 42 MPa) demonstrate the important, but dosage-sensitive, role of GQDs in cementitious systems (Figure 7 and Table 4). Although the benefit varied by type (liquid vs powder) and concentration, adding GQDs generally improved

https://doi.org/10.1021/acsomega.6c03084
ACS Omega XXXX, XXX, XXX−XXX

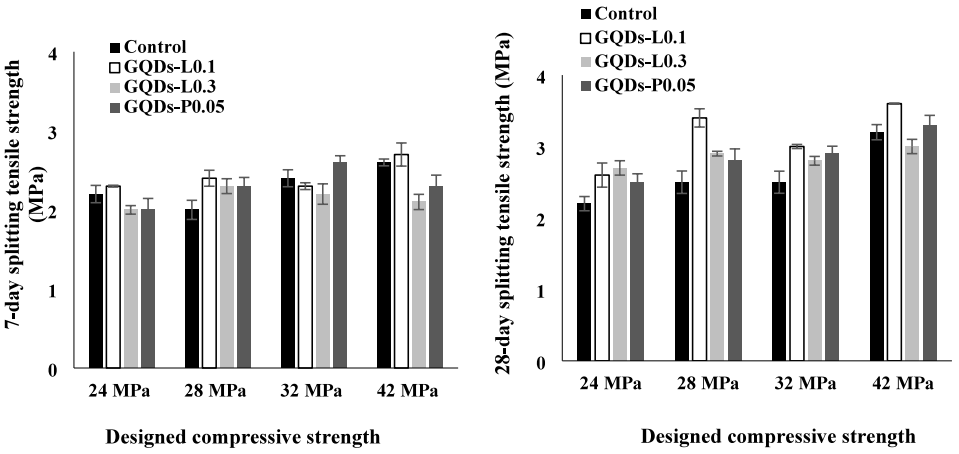

Figure 8. Results of splitting tensile strength for concrete with GQDs: (a) 7-day strength and (b) 28-day strength.

Table 5. Splitting Tensile Strength of Control and GQDs-Modified Concrete at 3, 7, and 28 Days[a]

strength class	age (days)	control (MPa)	GQDs-L0.1 (MPa)	GQDs-L0.3 (MPa)	GQDs-P0.05 (MPa)
24 MPa	7	2.2 ± 0.11	2.3 ± 0.01	2.0 ± 0.05	2.0 ± 0.14
	28	2.2 ± 0.10	2.6 ± 0.17	2.7 ± 0.10	2.5 ± 0.12
28 MPa	7	2.0 ± 0.12	2.4 ± 0.10	2.3 ± 0.09	2.3 ± 0.11
	28	2.5 ± 0.16	3.4 ± 0.13	2.9 ± 0.03	2.8 ± 0.17
32 MPa	7	2.4 ± 0.11	2.3 ± 0.04	2.2 ± 0.13	2.6 ± 0.08
	28	2.5 ± 0.15	3.0 ± 0.03	2.8 ± 0.06	2.9 ± 0.10
42 MPa	7	2.6 ± 0.04	2.7 ± 0.15	2.1 ± 0.10	2.3 ± 0.14
	28	3.2 ± 0.11	3.6 ± 0.01	3.0 ± 0.10	3.3 ± 0.14

[a]Data present the average value ± standard deviation.

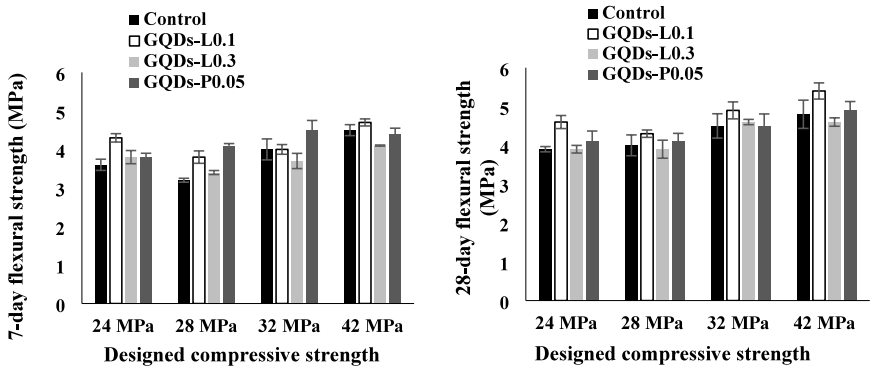

Figure 9. Results of flexural strength for concrete with GQDs: (a) 7-day strength and (b) 28-day strength.

strength development. The general pattern indicates that GQDs function as multifunctional nanoscale reactive sites that affect hydration chemistry and microstructural refinement, with slight early age improvements, greater acceleration effects at intermediate ages, and significant later-age increases.[40]

The gains were slight but noticeable after 3 days, especially in the weaker strength courses. The control mix in the 24 MPa concrete reached 21.6 MPa, but adding 0.1% liquid GQDs increased the strength to 25.2 MPa, a 17% improvement. Likewise, strength increased by over 20% in the 28 MPa class, from 19.4 MPa (control) to 23.2 MPa (L0.1%). While the 42 MPa class increased from 30.4 MPa (control) to 33.6 MPa (L0.1%), the 32 MPa class increased from 22.8 MPa (control) to 25.2 MPa (L0.1%) and 26.1 MPa (P0.05%). These findings are consistent with research on GNPs [39] and suggest that GQDs provide additional nucleation sites for the early precipitation of calcium silicate hydrate (C−S−H).[41] But the greater liquid dosage (0.3%) and powder form (0.05%) were less beneficial or inconsistent, suggesting that the advantages can be diminished at very early ages due to inadequate dispersion or particle agglomeration.[42,43]

Although gains differed by strength class, the GQDs effect on hydration rate became more pronounced at 7 days. While the 42 MPa mix went from 35.2 to 38.7 MPa with the same dosage, the 28 MPa concrete's compressive strength improved by 11%, from 30.4 MPa (control) to 33.8 MPa (L0.1%). These findings imply that GQDs improved hydration kinetics, leading to denser microstructures and more hydration products at this stage. Microstructural evidence for faster hydration was provided by TGA (Section 3.4.2), which showed higher levels of bound water and portlandite (CH) in GQDs mixes. The higher GQDs dosages (0.3% liquid and 0.05% powder) in the 24 and 32 MPa concretes, on the other hand, either underperformed or yielded insignificant benefits, indicating once more how crucial dosage

https://doi.org/10.1021/acsomega.6c03084
ACS Omega XXXX, XXX, XXX−XXX

Table 6. Flexural Strength of Control and GQDs-Modified Concrete at 3, 7, and 28 Days[a]

strength class	age (days)	control (MPa)	GQDs-L0.1 (MPa)	GQDs-L0.3 (MPa)	GQDs-P0.05 (MPa)
24 MPa	7	3.6 ± 0.15	4.3 ± 0.11	3.8 ± 0.17	3.8 ± 0.10
	28	3.9 ± 0.07	4.6 ± 0.17	3.9 ± 0.10	4.1 ± 0.27
28 MPa	7	3.2 ± 0.05	3.8 ± 0.16	3.4 ± 0.05	4.1 ± 0.05
	28	4.0 ± 0.27	4.3 ± 0.10	3.9 ± 0.23	4.1 ± 0.21
32 MPa	7	4.0 ± 0.27	4.0 ± 0.13	3.7 ± 0.20	4.5 ± 0.25
	28	4.5 ± 0.31	4.9 ± 0.22	4.6 ± 0.07	4.5 ± 0.31
42 MPa	7	4.5 ± 0.14	4.7 ± 0.09	4.1 ± 0.01	4.4 ± 0.15
	28	4.8 ± 0.36	5.4 ± 0.21	4.6 ± 0.11	4.9 ± 0.23

[a]Data present the average value ± standard deviation.

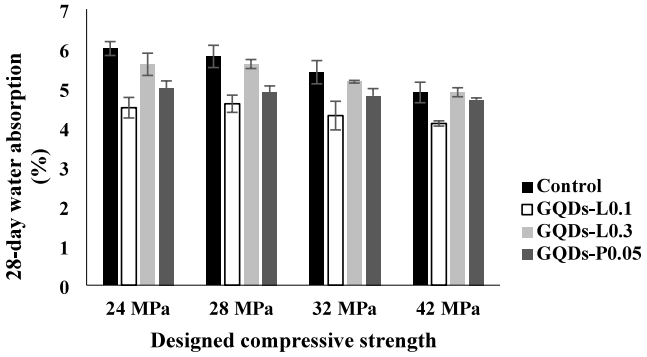

Figure 10. Results of water absorption for concrete with GQDs.

Table 7. Water Absorption of Control and GQDs-Modified Concrete[a]

strength class	control (%)	GQDs-L0.1 (%)	GQDs-L0.3 (%)	GQDs-P0.05 (%)
24 MPa	6.0 ± 0.18	4.5 ± 0.26	5.6 ± 0.28	5.0 ± 0.18
28 MPa	5.8 ± 0.28	4.6 ± 0.22	5.6 ± 0.11	4.9 ± 0.15
32 MPa	5.4 ± 0.29	4.3 ± 0.36	5.2 ± 0.03	4.8 ± 0.18
42 MPa	4.9 ± 0.26	4.1 ± 0.07	4.9 ± 0.11	4.7 ± 0.05

[a]Data present the average value ± standard deviation.

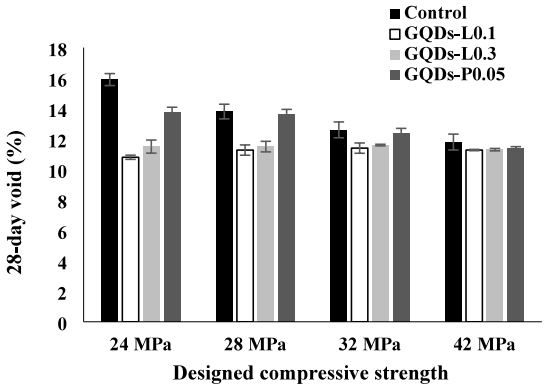

Figure 11. Porosity for concrete with GQDs.

Table 8. Porosity of Control and GQDs-Modified Concrete[a]

strength class	ontrol (%)	GQDs-L0.1 (%)	GQDs-L0.3 (%)	GQDs-P0.05 (%)
24 MPa	15.9 ± 0.39	10.8 ± 0.14	11.5 ± 0.43	13.7 ± 0.36
28 MPa	13.8 ± 0.48	11.3 ± 0.34	11.5 ± 0.35	13.6 ± 0.30
32 MPa	12.6 ± 0.52	11.4 ± 0.34	11.6 ± 0.05	12.4 ± 0.30
42 MPa	11.8 ± 0.52	11.3 ± 0.04	11.3 ± 0.08	11.4 ± 0.12

[a]Data present the average value ± standard deviation.

and dispersion are to effectiveness. These findings were also confirmed by the Raman results of pastes containing GQDs.[44]

The beneficial effects of GQDs were most noticeable by day 28, especially in the lower- and medium-strength classes. The GQDs-L0.1% mix produced 37.8 MPa, a significant 32% improvement over the control concrete's 28.6 MPa, placing it in the 24 MPa class. The 28 MPa concrete exhibited similar trends, increasing by 27% from 32.1 MPa (control) to 40.7 MPa (L0.1%). The 32 MPa control (34.6 MPa) grew to 37.1 MPa with L0.1%, while the 42 MPa control (44.5 MPa) increased to 47.1 MPa with L0.1%, demonstrating gains even in the higher strength blends. The long-term microstructural refinement is responsible for these improvements. GQDs concretes had lower total pore volumes (Section 3.4.1), especially in the mesopore (Type IV) range (10−50 nm), which has a direct impact on durability and strength.

One significant finding is that the 0.1% liquid GQDs continuously worked better than the 0.05% powder form and the higher 0.3% liquid dosage across all curative ages. For example, the 0.1% liquid form produced 37.8 MPa at 28 days in the 24 MPa concrete, while the larger dosage produced 33.9 MPa, and the powder produced only 29.5 MPa. This suggests that an ideal dosage threshold exists, beyond which aggregation and inadequate dispersion outweigh any potential advantages. Researchers have documented similar dose sensitivity for GO, with performance deteriorating at 0.08%.[45] It is important to note that the powder form performed well in some classes (e.g., 32 MPa at 3 days), suggesting that suprastructures with greater surface area might be useful under ideal conditions.

These outcomes are consistent with the research by Hong et al.[46] who found that concrete treated with GO showed increased strength due to faster hydration. The effect is particularly more noticeable in the case of GQDs because of their numerous oxygenated functional groups (e.g., −OH, −COOH), which operate as strong attractants for clinker phases like C_3S, C_2S, and C_3A. The precipitation of hydration products is accelerated by these phases, which are attracted to the nanoparticles' surfaces and serve as secondary hydration.[20]

In addition to providing nucleation sites, the high density of oxygen-containing functional groups on GQDs promoted the formation of a densely packed crystalline network within the matrix. This microstructural improvement enhanced stress transfer across the hardened composite, decreased pore connectivity, and lowered porosity. Moreover, vital cations like Ca^{2+}, Na^{+}, and K^{+} were drawn into the immediate micro-environment by the electronegative surfaces of GQDs. These ions further promoted the production of C−S−H, C-A−S-H, and ettringite (Aft) through chemical interactions with Al, Si, and SO_3 species. These phases coformed in the presence of water molecules, resulting in a compressed, tightly bonded matrix that can withstand both tensile and compressive pressures.

https://doi.org/10.1021/acsomega.6c03084
ACS Omega XXXX, XXX, XXX−XXX

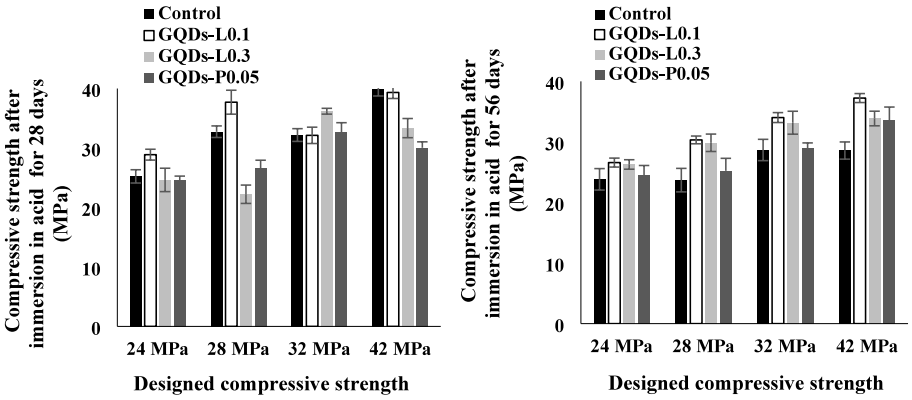

Figure 12. Results of resistance of acid attack for concrete with GQDs: (a) at 28 days and (b) at 56 days of immersion.

Table 9. Resistance of Acid Attack of Control and GQDs-Modified Concrete[a]

strength class	age (days)	control (MPa)	GQDs-L0.1 (MPa)	GQDs-L0.3 (MPa)	GQDs-P0.05 (MPa)
24 MPa	28-day immersion in acid	25.2 ± 1.12	28.9 ± 0.91	24.6 ± 1.97	24.6 ± 0.71
28 MPa		32.7 ± 0.97	37.7 ± 2.01	22.2 ± 1.54	26.6 ± 1.31
32 MPa		32.2 ± 1.07	32.1 ± 1.37	36.2 ± 0.49	32.6 ± 1.61
42 MPa		40.0 ± 1.21	39.3 ± 1.01	33.3 ± 1.61	30.1 ± 0.98
24 MPa	56-day immersion in acid	23.8 ± 1.77	26.6 ± 0.74	26.3 ± 0.78	24.5 ± 1.64
28 MPa		23.7 ± 1.94	30.3 ± 0.64	29.9 ± 1.44	25.2 ± 2.05
32 MPa		28.7 ± 1.76	34.0 ± 0.82	33.2 ± 1.89	28.9 ± 0.91
42 MPa		28.6 ± 1.42	37.2 ± 0.74	33.9 ± 1.21	33.6 ± 2.20

[a]Data present the average value ± standard deviation.

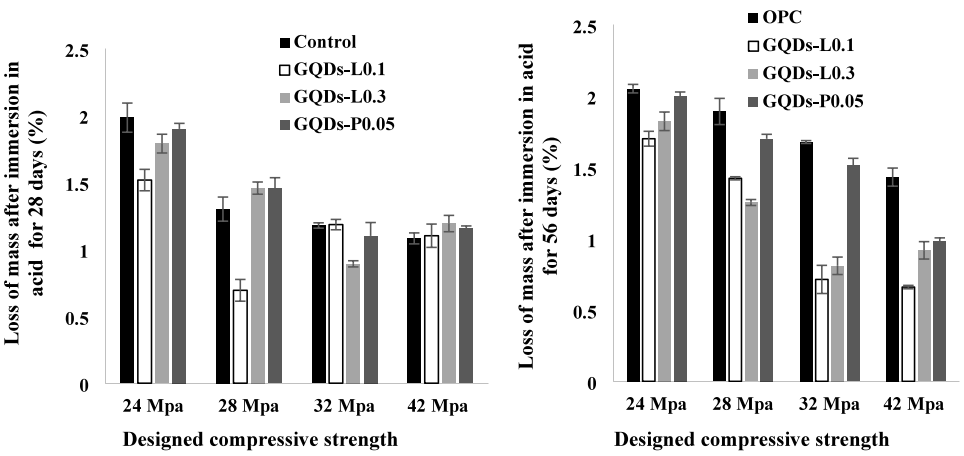

Figure 13. Loss of mass (%) of control and GQDs-modified concretes after immersion in acid solution: (a) 28-day exposure and (b) 56-day exposure.

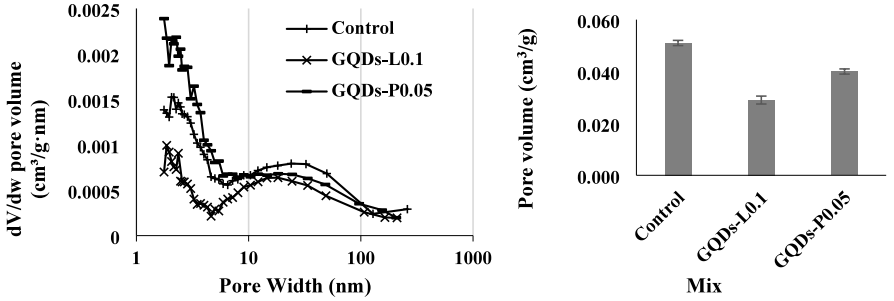

Figure 14. Nitrogen sorption analysis of GQDs-modified mixes: (a) pore size distribution curves showing Type IV isotherm behavior and (b) total pore volume comparison.

When combined, these findings support a three-phase mechanism for GQDs in concrete: (i) they function as nucleation agents at early ages, slightly speeding up hydration; (ii) they improve hydration kinetics at intermediate ages, as

https://doi.org/10.1021/acsomega.6c03084
ACS Omega XXXX, XXX, XXX−XXX

Table 10. Pore Structure of Cement Composites Containing GQDs

mix	surface area (m^2/g)	pore volume (cm^3/g)
control	16.82	0.051
GQDs-L0.1	9.54	0.029
GQDs-P0.05	15.39	0.040

shown by TGA and XRD; and (iii) at later ages, they refine pore structure and densify the ITZ, as shown by BET and FESEM. The current work reports gains of up to 32% compared with previous studies on GNPs and GO, where improvements typically ranged from 10−17%,[3,12,42] indicating superior efficiency of quantum-scale additives.

3.2.2. Splitting Tensile Strength. Significant information about how GQDs enhance the tensile behavior of concrete was gained from the splitting tensile strength data of the control and GQDs-modified concrete across various strength classes at 7 and 28 days (Figure 8andTable 5). Splitting tensile strength emphasizes the material's resistance to crack initiation and propagation, a property heavily influenced by matrix-aggregate bonding, microstructural refinement, and the presence of nanomaterials. Such data contrast with compressive strength, which primarily reflects bulk resistance to axial loads.

At 7 days, the control mix's tensile strength in the 24 MPa strength class was 2.2 MPa; however, GQDs-L0.1 slightly increased the value to 2.3 MPa. GQDs-L0.3 and GQDs-P0.05, on the other hand, recorded somewhat lower values (2.0 MPa each), indicating that greater dosages or powdered forms of GQDs might not disperse effectively enough to improve fracture resistance at early ages. But after 28 days, there was a noticeable improvement: GQDs-L0.1 rose to 2.6 MPa, and GQDs-L0.3 reached 2.7 MPa, which was around 20−23% higher than the control. Strength was enhanced to 2.5 MPa even with GQDs-P0.05.

Compared with the control (2.0 MPa), the 7-day results indicate an initial rise in the 28 MPa strength class for all GQDs-modified mixtures. While both GQDs-L0.3 and GQDs-P0.05 recorded 2.3 MPa, GQDs-L0.1 achieved the largest gain at 2.4 MPa. The benefits became more noticeable after 28 days: GQDs-L0.1 increased by an astounding 36% to 3.4 MPa, whereas the control mix only managed 2.5 MPa. Significant improvements were also seen in GQDs-L0.3 (2.9 MPa) and GQDs-P0.05 (2.8 MPa). According to these findings, the 28 MPa system's bond strength and microcrack resistance were most improved by a modest liquid GQDs dosage of 0.1%.

In addition, the 32 MPa strength class values at 7 days varied somewhat: GQDs-P0.05 increased slightly to 2.6 MPa, while the control (2.4 MPa) remained similar to GQDs-L0.1 (2.3 MPa) and GQDs-L0.3 (2.2 MPa). The function of GQDs became clearer after 28 days: GQDs-L0.1 and GQDs-P0.05 rose to 3.0 and 2.9 MPa, respectively, while GQDs-L0.3 trailed slightly behind at 2.8 MPa. The control mix achieved 2.5 MPa (as discussed in Section3.4.4, in addition to the microstructure investigations). Moreover, in the 42 MPa strength class, the control mix showed 2.6 MPa at 7 days, increasing to 3.2 MPa at 28 days. When GQDs-L0.1 was added, early age strength rose to 2.7 MPa and then to 3.6 MPa at 28 days, the highest of all mixes and an improvement of around 12.5% over the control. Curiously, GQDs-L0.3 reached 3.0 MPa at 28 days despite underperforming at 7 days (2.1 MPa), presumably as a result of agglomeration effects at higher doses in low w/c mixes. Additionally, GQDs-P0.05 contributed positively, reaching 3.3 MPa after 28 days. These findings demonstrate that the effectiveness of GQDs in high-strength concrete with reduced porosity depends heavily on appropriate dispersion, with the best results obtained with moderate liquid dosages.

The overall pattern across all strength classes shows that GQDs enhance splitting tensile strength more effectively at 28 days than at 7 days, underscoring their long-term role in matrix densification and improved resistance to crack initiation and propagation. The most effective method for improving tensile characteristics was consistently found to be liquid GQDs at a

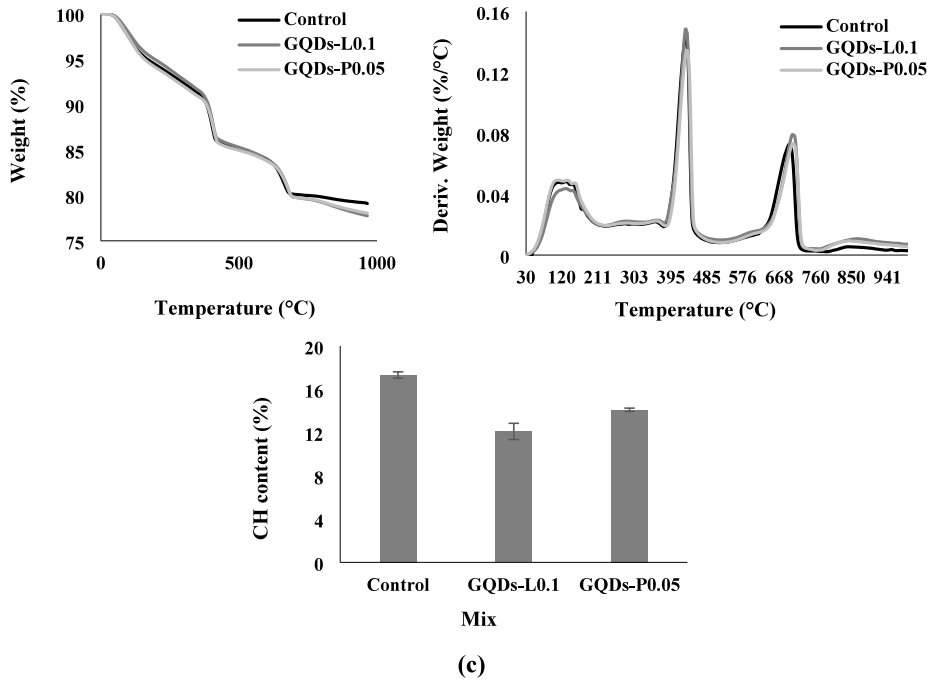

Figure 15. (a) TGA thermograms, (b) DTG thermograms, and (c) CH content of GQDs-modified mixes.

https://doi.org/10.1021/acsomega.6c03084
ACS Omega XXXX, XXX, XXX−XXX

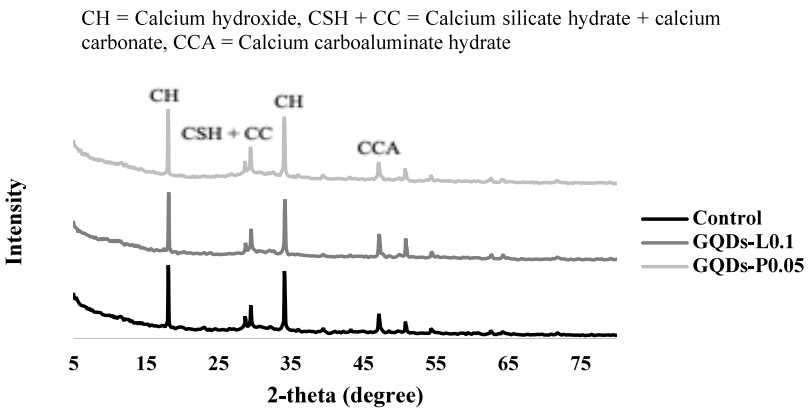

Figure 16. XRD patterns of GQDs-modified mixes at 28 days of curing.

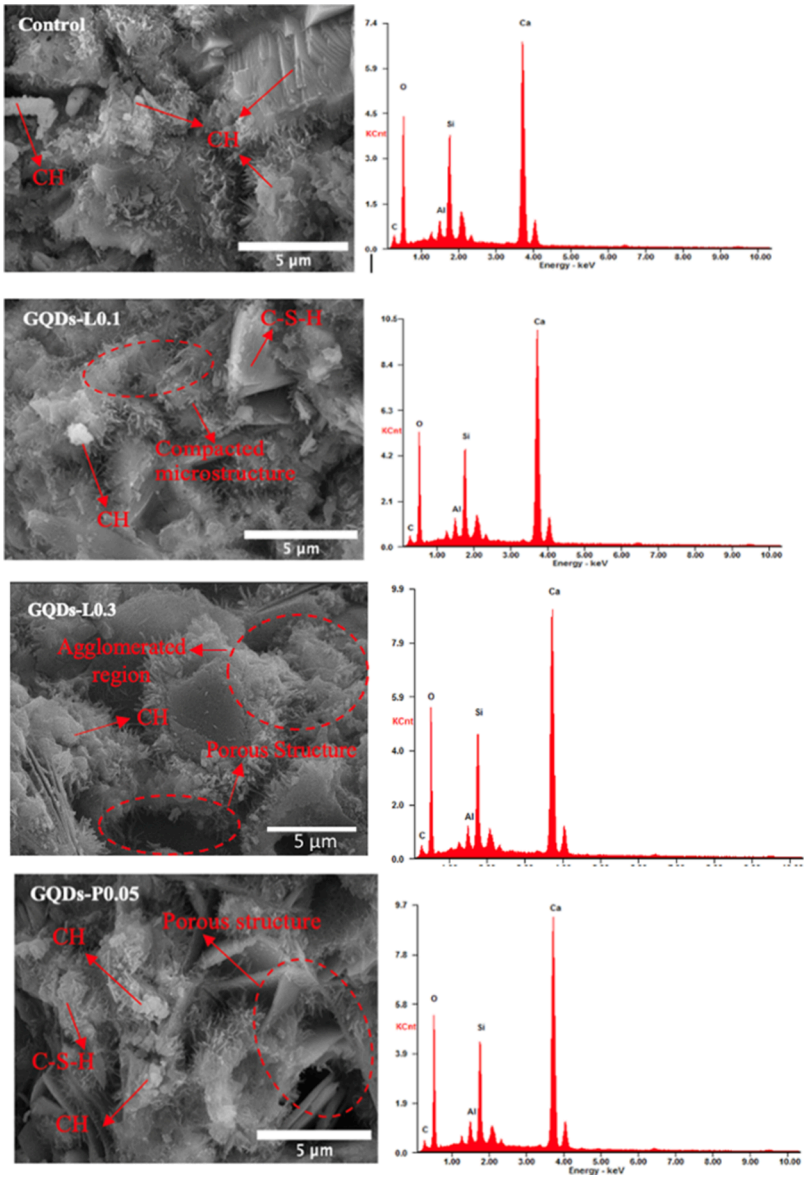

Figure 17. FESEM micrographs (left) and EDS elemental spectra (right) obtained from fractured surface of control, GQDs-L0.1, GQDs-L0.3, and GQDs-P0.05 samples.

dosage of 0.1% (GQDs-L0.1), especially in the 28 and 42 MPa classes. Even though gains are still noticeable at later curative stages, early age agglomeration effects may offset benefits at higher dosages (0.3%). At 32 and 42 MPa, where proper dispersion probably lessened agglomeration problems, powdered GQDs showed modest but consistent gains.

https://doi.org/10.1021/acsomega.6c03084
ACS Omega XXXX, XXX, XXX−XXX

Table 11. Atomic Composition of the Control and GQDs-Modified Cement Composites

	atomic %				
sample	C	O	Al	Si	Ca
control	5.2	58.0	1.5	8.8	26.5
GQDs-L0.1	4.5	56.7	1.8	8.4	28.6
GQDs-L0.3	4.7	56.8	1.8	8.3	28.4
GQDs-P0.05	4.6	56.8	1.8	8.5	28.3

As explained in the previous section, GQDs' capacity to function as ion attractors and hydration accelerators, simultaneously accounts for their interaction with hydration chemistry. The quantum dot scale, in contrast to larger graphene derivatives, ensures a more even distribution within the cementitious matrix, reducing the risk of agglomeration and enhancing nanoscale interactions. These outcomes include better mechanical performance, a finer microstructure, and enhanced hydration kinetics. In the end, the addition of GQDs results in a cementitious system that is stronger, more resilient, and more long-lasting.[36]

According to earlier research, graphene derivatives increase tensile resistance through microstructure refinement, improved ITZ bonding, and nanoscale crack-bridging effects.[47] These results are consistent with those findings. Specifically, the combination of GQDs and cement hydration products likely promotes denser gel formation and stronger aggregate−matrix interactions, thereby enhancing tensile strength. For solid GQDs, it is believed that the heat of hydration can break down the suprastructure of GQDs, enhancing the particles' dispersion mechanism.

3.2.3. Flexural Strength. The flexural strength results for the control and GQDs-modified concretes at 7 and 28 days are shown in Figure 9 and Table 6. Flexural strength is particularly sensitive to microcrack propagation and the ability of the matrix to bridge cracks under bending stresses. The results demonstrate that GQDs improve flexural strength across all strength classes, with the extent of improvement depending on dosage, curing age, and concrete grade. At 7 days in the 24 MPa strength class, the control mix achieved a flexural strength of 3.6 MPa, while the inclusion of GQDs-L0.1 increased it to 4.3 MPa (19% improvement). GQDs-L0.3 and GQDs-P0.05 also provided moderate enhancements (3.8 MPa each). By 28 days, GQDs-L0.1 maintained the highest flexural strength at 4.6 MPa, compared to 3.9 MPa for the control. Even the powdered form (4.1 MPa) showed a noticeable improvement, indicating that at lower strength grades, GQDs-L at modest dosages is particularly effective in enhancing crack resistance. Furthermore, in the 28 MPa strength class, the control mix recorded 3.2 MPa, which increased to 3.8 MPa with GQDs-L0.1 and to 4.1 MPa with GQDs-P0.05. By day 28, the control reached 4.0 MPa, while GQDs-L0.1 and GQDs-P0.05 reached 4.3 and 4.1 MPa, respectively. These results suggest that both liquid and powdered GQDs can significantly improve bending resistance in medium-strength systems.

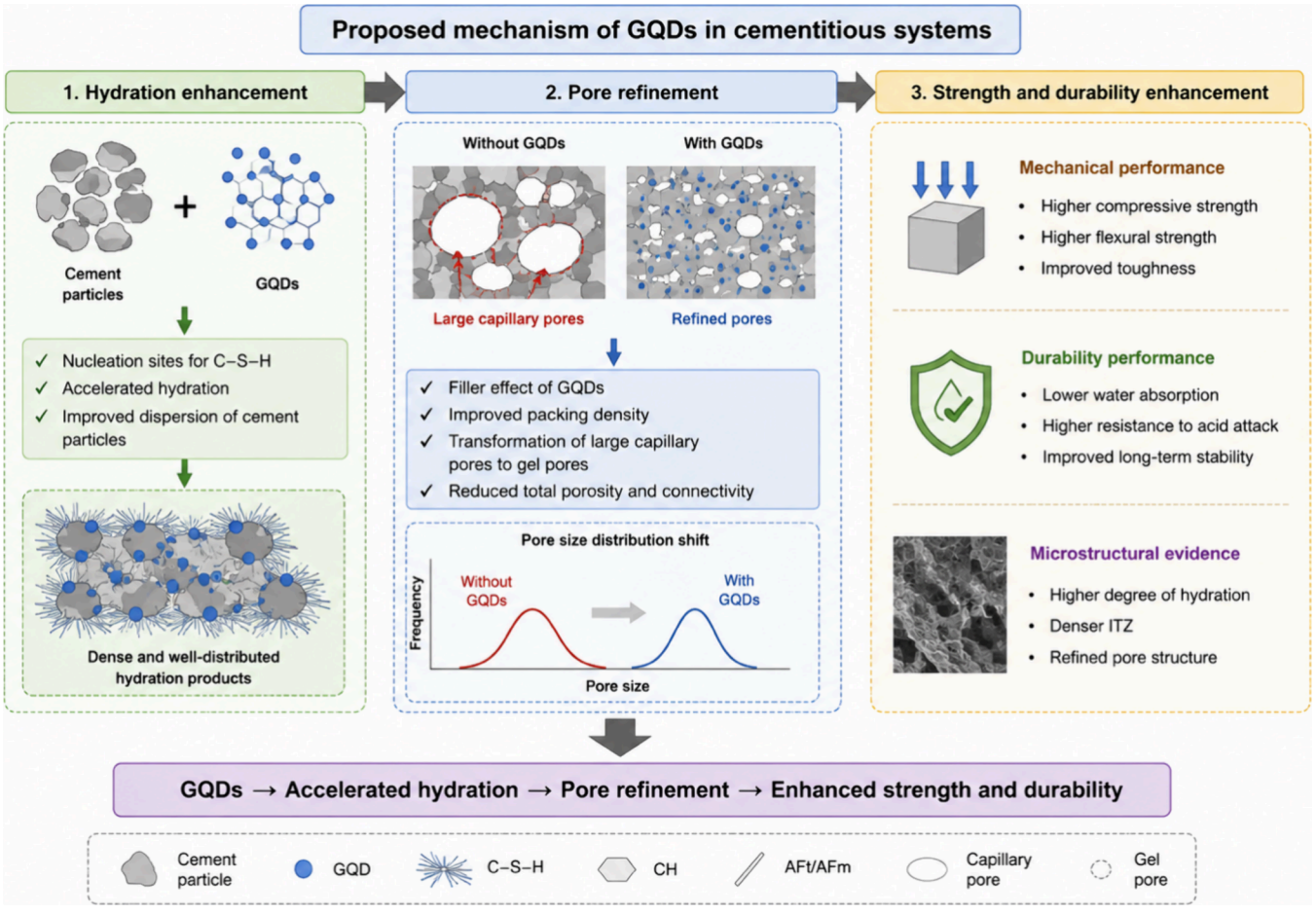

Figure 18. Schematic illustration of the proposed mechanism of GQDs in cementitious systems.

https://doi.org/10.1021/acsomega.6c03084
ACS Omega XXXX, XXX, XXX−XXX

Additionally, at 7 days in the 32 MPa strength class, the control reached 4.0 MPa, comparable to GQDs-L0.1 (4.0 MPa), whereas GQDs-P0.05 showed the greatest improvement, reaching 4.5 MPa. By 28 days, flexural strength increased further to 4.9 MPa with GQDs-L0.1 and 4.6 MPa with GQDs-L0.3, compared to 4.5 MPa for the control. Nevertheless, at 7 days in the 42 MPa strength class, the control exhibited 4.5 MPa, while GQDs-L0.1 slightly improved this to 4.7 MPa. However, GQDs-L0.3 underperformed at 4.1 MPa, likely due to nanoparticle agglomeration at higher dosages in low w/c systems. By 28 days, GQDs-L0.1 achieved the highest flexural strength of 5.4 MPa (12.5% higher than the control at 4.8 MPa). GQDs-L0.3 (4.6 MPa) and GQDs-P0.05 (4.9 MPa) also performed better than the control, confirming that well-dispersed GQDs can effectively enhance fracture resistance even in high-strength matrices.

Across all strength classes, results consistently show that GQDs enhance flexural strength more at 28 days than at 7 days, aligning with the observed trends in compressive and splitting tensile strength. These improvements confirm that GQDs increase strength and enhance the structural resilience of concrete.[48,49] Optimal performance was observed at a liquid dosage of 0.1%, while higher dosages (0.3%) sometimes reduced efficiency due to agglomeration, particularly at early ages. Long et al.[50] and Lv et al.[20] reported significant increases in the flexural resistance of GO- and GNP-modified cement composites, attributing the gains to nanoscale crack bridging and microstructural refinement. Similarly, Mohammed et al.[17] demonstrated that GNPs enhanced both splitting tensile and flexural strength due to ITZ densification. More recently, Wang et al.[51] further explained that oxygenated functional groups on graphene derivatives act as catalyzing additional hydrate formation. These studies support the current findings and highlight the role of GQDs as effective nanoscale reinforcements in cementitious systems.

Microstructural observations (Section 3.4.4) revealed a denser and more compact matrix, while BET analysis (Section 3.4.1) showed greater mesopore refinement in the liquid-GQDs systems. In addition, TGA (Section 3.4.2) and XRD (Section 3.4.3) analyses indicated enhanced hydration product formation and reduced CH content. Collectively, these findings suggest that liquid GQDs may promote more effective interfacial interactions during hydration. However, as no direct dispersion stability or agglomeration analysis was conducted, this interpretation should be considered indirect.

3.3. Durability Studies

3.3.1. Water Absorption. The water absorption test provides useful information on the pore structure and permeability of concrete, both of which directly influence long-term durability. As shown in Figure 10 and Table 7, the incorporation of GQDs consistently reduced water absorption across all strength classes compared to the control mixes. For instance, in the 24 MPa class, the control exhibited a water absorption of 6.0%, whereas mixes containing GQDs-L0.1 and GQDs-P0.05 showed reductions to 4.5% and 5.0%, respectively. A similar trend was observed for higher-strength classes, with the 42 MPa mix showing the lowest absorption value (4.1%) upon modification with GQDs-L0.1. This pattern highlights that, even at relatively low dosages, GQDs can effectively refine pore connectivity and limit the ingress of external fluids.

The reduction in water absorption can be attributed to the nanofilling of GQDs within the cementitious system. The data also reveal subtle differences between liquid and powdered forms of GQDs. Liquid-based GQDs (L0.1) demonstrated superior performance in lowering water absorption compared to powdered GQDs (P0.05). This finding can be explained by the better dispersion characteristics of liquid GQDs, which minimize the risk of agglomeration and ensure a more homogeneous distribution throughout the cement matrix. In contrast, powdered GQDs are more prone to clustering, which may reduce their effectiveness in blocking pore networks. Similar findings have been reported by Qureshi and Panesar [40], who found that graphene derivatives improved pore refinement, but dispersion quality critically influenced the magnitude of the improvement.

Another noteworthy observation is that the beneficial effect of GQDs becomes more pronounced as the compressive strength class increases. For instance, the percentage reduction in water absorption from control to GQDs-L0.1 is approximately 25% for the 24 MPa mix, whereas for the 42 MPa mix it is closer to 16%. This aspect may be due to the inherently denser microstructure of higher-grade concretes, which limits the relative margin for further improvement. Nevertheless, even within high-strength mixes, GQDs impart measurable durability gains, underscoring their robustness as a nanomodification strategy. Reduced water absorption directly correlates with lower risks of acid attack, as the transport of aggressive agents into the concrete matrix is governed by fluid permeability. By effectively reducing water absorption, GQDs extend the service life of concrete structures in harsh environments. Previous reports[52,53] have shown that graphene derivatives significantly improve impermeability and reduce permeability coefficients of cementitious composites, which aligns with these findings.

The water absorption results demonstrate that GQDs play a crucial role in densifying the pore structure and enhancing concrete's impermeability. This effect is driven by their nanofilling ability, hydration acceleration, and electrostatic interactions that attract cations into the gel phase. The improved microstructural compactness validates the mechanical improvements discussed earlier and emphasizes the potential of GQDs to create concretes with superior long-term durability. Durability is inherently linked to the pore structure of concrete. Thus, in addition to water absorption, porosity, acid resistance, and BET analysis were further evaluated to develop a comprehensive understanding of the influence of GQDs on the long-term performance of cementitious composites.

3.3.2. Porosity. As shown in Figure 11and Table 8, the porosity results of control and GQDs-modified concretes show a distinct trend of pore structure refinement with the addition of GQDs. The control had the highest porosity (15.9%) in the 24 MPa mix, while the addition of GQDs-L0.1 reduced porosity to 10.8%, a reduction of about 32%. Similarly, when GQDs-L were added to the 28 and 32 MPa mixtures, the porosity values dropped from 13.8% to 11.3% and from 12.6% to 11.4%, respectively. Porosity decreased from 11.8% in the control to 11.3% in the GQDs-modified concretes in the highest strength class (42 MPa), demonstrating the trend. By reducing void content across several strength classes, the results consistently show that GQDs can densify the cementitious microstructure. Concrete becomes denser and less permeable as a result of these C−S−H and C-A−S-H gel occupations of pore spaces and microstructure refinement. Prior research on GO and other graphene derivatives has documented this synergistic impact, with gel formation leading to decreased porosity and microstructural densification.[52] Interestingly, the lower-strength class

https://doi.org/10.1021/acsomega.6c03084
ACS Omega XXXX, XXX, XXX−XXX

(24 MPa) experienced the greatest decrease in porosity, while the relative improvements at higher-strength classes decreased. This is because higher-grade concretes, which already have lower baseline porosity, inherently have a denser microstructure. Because of this, even little improvements at this scale can greatly increase resistance to durability-related deterioration processes like acid attack, even though the absolute reductions in high-strength mixtures were modest (for example, from 11.8% to 11.3% in the 42 MPa class).

The water-absorption data presented in Section 3.3.1 are highly consistent with these porosity findings. Both metrics confirm that GQDs densify the ITZ and refine the pore structure, thereby lowering the cementitious matrix's permeability. Improved durability is a direct result of the interaction between decreased absorption and porosity, as demonstrated by the BET surface area studies (Section 3.4.1). These findings collectively provide a thorough understanding of how GQDs maximize pore structure to prolong service life in demanding conditions.

3.3.3. Acid Attack Resistance. The results of the acid resistance test, illustrated in Figure 12 and Table 9, demonstrate that the influence of GQDs on the acid resistance of concrete depends strongly on the dosage, physical form, and concrete strength class. Although several GQDs-modified mixtures exhibited improved durability compared with the control concretes after immersion in an acidic environment, the enhancement was not consistently observed for all mixtures. In particular, some mixtures containing higher dosages of liquid GQDs or powdered GQDs exhibited lower retained compressive strengths than the corresponding control concretes, indicating that the effectiveness of GQDs is highly dependent on optimized incorporation conditions.

After 28 days of acid immersion, the most significant improvement was observed in the mixtures containing low-dosage liquid GQDs (GQDs-L0.1). For example, in the 24 MPa concrete, the retained compressive strength increased from 25.2 MPa in the control mixture to 28.9 MPa in GQDs-L0.1, corresponding to an increase of approximately 15%. Similarly, the 28 MPa mixture improved from 32.7 to 37.7 MPa. However, not all GQDs-modified concretes outperformed the control mixtures. In the 28 MPa class, GQDs-L0.3 and GQDs-P0.05 exhibited retained strengths of 22.2 and 26.6 MPa, respectively, both lower than the control value. Likewise, in the 42 MPa class, GQDs-L0.3 and GQDs-P0.05 showed lower strengths of 33.3 and 30.1 MPa compared with the control concrete (40.0 MPa). These results suggest that increasing the GQDs dosage or using powdered GQDs does not necessarily enhance acid resistance. The mass loss results presented in Figure 13a further support these findings. The control mixtures exhibited mass losses ranging from 1.08 to 1.98%, whereas several GQDs-L0.1 mixtures showed lower values, indicating reduced surface deterioration during acid exposure. In contrast, some mixtures containing GQDs-L0.3 and GQDs-P0.05 exhibited mass losses comparable to the control concrete.

After 56 days of immersion, the differences between the mixtures became more evident. The GQDs-L0.1 mixtures generally maintained better long-term resistance against acid attack. For instance, the retained compressive strength of the 28 MPa concrete increased from 23.7 MPa in the control mixture to 30.3 MPa in GQDs-L0.1, while the 42 MPa concrete increased from 28.6 to 37.2 MPa. Correspondingly, the mass losses (Figure 13b) decreased from 1.89% to 1.42% for the 28 MPa mixture and from 1.43% to 0.66% for the 42 MPa mixture. Although GQDs-L0.3 demonstrated improved resistance in some mixtures after prolonged exposure, the performance of GQDs-P0.05 remained inconsistent, especially in lower-strength concretes.

The deterioration observed in certain GQDs-modified mixtures may be associated with nanoparticle agglomeration and nonuniform dispersion at higher dosages or in powdered form. Excessive GQDs content could lead to localized defects, weak interfacial regions, or microvoids within the cement matrix, which may facilitate acid ingress and accelerate the degradation of hydration products during prolonged exposure. Furthermore, the effectiveness of GQDs appears to depend on the initial compactness of the concrete matrix. In lower-strength concretes, moderate GQDs incorporation may contribute to pore refinement and reduced permeability, whereas excessive nanoparticle addition in denser matrices may disturb the optimized microstructure and reduce the beneficial effect.

The improved performance observed in the optimized GQDs-L0.1 mixtures is likely related to microstructural densification and reduced permeability, which limited the penetration of aggressive ions and slowed the degradation of the cementitious matrix during acid exposure. Similar findings have been reported by Hong et al.,[46] who observed that GO and related nanostructures promote durable gel formation and delay acid-induced degradation by enhancing microstructural packing. The improved mechanical integrity observed in Sections 3.2.1−3.2.3 complements these findings, as denser matrices resist microcracking and acid infiltration more effectively. The coherence between these findings and those from the water absorption and porosity tests strongly supports the conclusion that GQDs enhance long-term durability through synergistic physical and chemical mechanisms. This conclusion is further supported by BET surface analysis (Section 3.4.1), which reveals nanostructural densification responsible for the improved acid resistance of GQDs-modified concretes.

3.4. Microstructure Characterization

The microstructural analyses are conducted using small pieces collected from fractured 28-day compressive strength specimens of the 28 MPa concrete mixtures, including control, GQDs-L0.1, GQDs-L0.3, and GQDs-P0.05. The 28 MPa strength class was selected because it showed the most representative variation in performance among the mixtures, including both the improved behavior of GQDs-L0.1 and the noticeable performance reduction of GQDs-L0.3 and GQDs-P0.05 compared with the control concrete.

3.4.1. BET Isotherm Analysis. The nitrogen adsorption isotherm and corresponding pore volume distributions of the Control, GQDs-L0.1, and GQDs-P0.05 mixes are shown in Figure 14, with the pore structure parameters summarized in Table 10. The GQDs-L0.1 mixture shows a pronounced reduction in pore volume across the mesopore range (2−50 nm), particularly around 10 nm, where capillary pores dominate transport. This seems to have a similar range to GQDs particles. The total pore volume decreased from 0.051 cm^3/g in the control to 0.029 cm^3/g in GQDs-L0.1, representing that the 43% reduction in pore volume confirms GQDs regulate mesopore formation rather than merely filling voids. The specific surface area also decreased from 16.82 to 9.54 m^2/g, indicating a more refined, less accessible internal pore network. This microstructural densification aligns well with the reduced water absorption and porosity reported in Section3.3, as well as with the enhanced mechanical and acid-resistance performance. On

https://doi.org/10.1021/acsomega.6c03084
ACS Omega XXXX, XXX, XXX−XXX

the other hand, the GQDs-P0.05 mix showed an intermediate behavior, with a pore volume of 0.040 cm^3/g and a surface area of 15.39 m^2/g. While improved relative to the control, its performance was less pronounced than that of the liquid GQDs. This suggests that the dispersion state plays a crucial role.

BET analysis confirms that GQDs, particularly in their liquid form at 0.1% dosage, significantly refine the mesoporous structure (Type IV) of cement composites. This nanoengineering effect provides strong microstructural evidence of the enhanced durability and mechanical performance of GQDs-modified concrete.[54−57] These BET results clearly demonstrate that the significant mesopore refinement induced by GQDs is directly associated with the observed improvements in durability, reduced water absorption, enhanced acid resistance, and higher mechanical strength. This microstructural evidence provides a strong foundation for the overall interpretation of GQDs' role in cementitious systems, which will be further elaborated in Section3.4.4.

3.4.2. Thermogravimetric Analysis (TGA). TGA was used to determine the amount of CH present in the control and GQDs-modified mixes. The observed phases are identified by presenting the results as derivative thermogravimetric (DTG) curves. The peak at roughly 140 °C indicates approximately amorphous C−S−H, the peak at roughly 190 °C indicates the microcrystalline portion of C−S−H, and the peaks at 640 and 690 °C are caused by the breakdown of crystalline and amorphous $CaCO_3$, respectively. Figure 15a shows the TGA thermograms, which indicate that CH was detected between 415 and 475 °C.[58] When GQDs are added, the peak describing the CH phase becomes sharper, as can be observed, indicating that the CH phases of the GQDs-modified mix are highly crystallized in comparison to the control. A steady rise in the $CaCO_3$ peaks and a slight drop in the C−S−H peak are also seen in the figure. This could be because the − COOH group reacts with some CH to generate calcium carboaluminate hydrate, as shown in Figure 15b, which shows the DTG thermograms. Additionally, due to the reinforcing effect of the GQDs, all steps characterizing the CH phases of the prepared GQDs-modified mixes are shifted relative to the control mix (without GQDs), confirming the high thermal stability of the hydration products.[47,59] The following equation was used to determine the quantity of CH:

$$CH\% = WL_{CH}(\%) \times MW_{CH}/MW_{H}$$

WL_{CH} denotes the mass loss due to the breakdown of $_{CH}$, while the molecular weights of CH (74.01 g/mol) and H_2O (18 g/mol) are represented by MW_{CH} and MW_{H}, respectively.[60]Fig-Figure 15c shows the CH content of the control mix and the GQDs-modified mixes. The control mix has roughly 12% CH. GQDs-L0.1 has decreased the CH content because of their strong chemical reactivity, which promotes the formation of calcium carboaluminate hydrates $3CaO.Al_2O_3.CaCO_3.11H_2O$ (chemical consumption, not dilution). Additionally, it is evident that at GQDs-P0.05, the CH begins to rise again, despite the fact that its quantity in all mixes remains lower than in the control. This could be because it is difficult to uniformly distribute GQDs throughout the cement matrix, or because GQDs agglomerate in concrete containing 0.05% GQDs.

3.4.3. X-ray Diffraction (XRD) Analysis. XRD analysis was carried out to identify the crystalline phases present in the control, GQDs-L0.1, and GQDs-P0.05 mixes, as shown in Figure 16. The detected phases are the usual cement hydrates: C−S−H, CH, and calcium carboaluminate hydrate.[47] The GQDs-L0.1 mix shows a notable reduction in CH peak intensity, accompanied by increased intensities of C−S−H and calcium carboaluminate hydrate peaks. Meaningly, suppression of CH peaks indicates a shift in hydration equilibrium toward thermodynamically stable C-(A)−S-H phases. For the GQDs-P0.05 mix, a moderate increase in calcium carboaluminate hydrate peaks was observed, although less pronounced than with the liquid GQDs. The formation and increase of the calcium carboaluminate hydrate phase is particularly significant. These hydrates are known to enhance the dimensional stability and chemical resistance of cement pastes, thereby improving the durability of the hardened matrix.

The combined TGA/XRD and BET results provide evidence that changes in hydration products and pore structure are associated with the enhanced mechanical performance of GQDs-modified systems. TGA analysis revealed a reduction in CH content in the GQDs-modified mixtures, while XRD results showed enhanced formation of C−S−H and C−A−S−H phases. The reduction in CH alongside increased amorphous hydration products further suggests partial consumption of CH through secondary reactions, contributing to the formation of more stable hydrate phases and a denser cementitious network. These findings indicate that GQDs promoted hydration reactions and modified the hydration pathway toward the formation of additional binding products. The increased generation of hydration products subsequently refined the pore structure, as confirmed by BET analysis showing a substantial reduction in mesopore volume. The resulting densified microstructure reduced pore connectivity and enhanced matrix compactness, contributing to the observed improvements in compressive strength, durability, and acid resistance. Therefore, the mechanical enhancement is not solely associated with a filler effect, but also with hydration-pathway modulation and microstructural refinement induced by GQDs.

3.4.4. FESEM-EDS Analysis. The improvement in the mechanical and durability properties of the GQDs-modified cement composites can primarily be attributed to microstructural refinement. The FESEM-EDS examination (Figure 17) presents clear microstructural distinctions between the control mix and GQDs-containing samples. In the GQDs-L0.1 mix, a denser matrix with more crystalline features is observed. The voids within the cement matrix are effectively filled by the newly formed C−S−H gels and crystalline hydrates induced by the 0.1% GQDs addition. This densification results in enhanced strength and durability compared to the control specimen. The microstructure shows that well-dispersed liquid GQDs accelerate hydration and the formation of compact, cohesive gels. Conversely, the GQDs-L0.3 and GQDs-P0.05 specimen exhibits numerous fine, needle-like precipitates distributed closely throughout the matrix. These acicular formations are indicative of delayed ettringite formation, potentially associated with carbonation due to excess CO_2 exposure. Such microstructural irregularities can increase porosity and impair mechanical integrity, aligning with trends reported by[36] for similar cementitious systems.

The corresponding EDS elemental analysis results (Table 11) further support these observations. The calcium content is slightly higher in the GQDs-L0.1 sample than in the control, correlating with its higher proportion of crystalline hydration products. The GQDs-L0.3 and GQDs-P0.05 mix, on the other hand, shows higher levels of oxygen and carbon, suggesting carbonation and less effective hydration.[61] The minimal free carbon and higher calcium concentration detected in the GQDs-

https://doi.org/10.1021/acsomega.6c03084
ACS Omega XXXX, XXX, XXX−XXX

L0.1 sample imply more complete hydration reactions and limited carbonation, consistent with its superior mechanical and durability performance. Figure 18 illustrates the proposed mechanism of GQDs in cementitious systems based on the BET, TGA, XRD, and SEM results obtained in this study.

4. CONCLUSIONS

This study investigated the influence of graphene quantum dots (GQDs) on the mechanical performance, durability, and microstructural behavior of concrete across multiple strength classes. The results demonstrated that GQDs, particularly liquid-form GQDs at 0.1% dosage (GQDs-L0.1), significantly enhanced the overall performance of concrete systems.

The major scientific contributions and findings of this study are summarized as follows:

- GQDs significantly improved the compressive, splitting tensile, and flexural strengths of concrete across different strength classes. At 28 days, the compressive, splitting tensile, and flexural strengths increased by up to 32%, 36%, and 18%, respectively, compared with the control mixtures.
- GQDs enhanced durability performance by reducing water absorption and porosity by approximately 25% and 32%, respectively, while also improving acid resistance. After acid immersion, the GQDs-modified concrete exhibited up to 28% higher residual compressive strength and reduced deterioration compared with the control mixture.
- BET analysis revealed an approximately 43% reduction in mesopore volume, confirming that GQDs actively regulate pore structure refinement rather than acting solely as inert fillers.
- Combined BET, TGA, XRD, and FESEM-EDS analyses established a mechanistic relationship between hydration enhancement, mesopore refinement, and improved mechanical and durability performance.
- Liquid-form GQDs exhibited superior performance compared with powder-form GQDs, emphasizing the importance of nanoparticle dispersion and homogeneous interaction within the cementitious matrix.
- This study establishes a structure−property relationship linking GQD-induced hydration-pathway modulation and microstructural densification with enhanced concrete performance across multiple strength classes.

Overall, the findings demonstrate the strong potential of well-dispersed GQDs for developing next-generation high-performance and durable cementitious materials. Future studies should focus on long-term durability under real environmental conditions and the synergistic interaction between GQDs and supplementary cementitious materials for low-carbon concrete applications.

■ ASSOCIATED CONTENT

Data Availability Statement

The data supporting this study are available within the manuscript.

■ AUTHOR INFORMATION

Corresponding Author

Lapyote Prasittisopin − *Center of Excellence for Green Tech in Architecture, Department of Materials Science, Faculty of Science, Chulalongkorn University, Bangkok 10330, Thailand*; orcid.org/0000-0003-4860-7357; Email: lapyote.p@chula.ac.th

Authors

Thwe Thwe Win − *Department of Architecture, Faculty of Architecture and Center of Excellence for Green Tech in Architecture, Department of Materials Science, Faculty of Science, Chulalongkorn University, Bangkok 10330, Thailand*

Peem Nuaklong − *Research Unit in Sciences and Innovative Technologies for Civil Engineering Infrastructures, Department of Civil Engineering, Thammasat School of Engineering, Faculty of Engineering, Thammasat University, Pathumthani 12120, Thailand*

Jintara Lawongkerd − *Research Unit in Advanced Mechanics of Solids and Vibration, Department of Civil Engineering, Faculty of Engineering, Thammasat School of Engineering, Thammasat University, Pathum Thani 12120, Thailand*

Fahim Ullah − *School of Science, Engineering and Digital Technologies, University of Southern Queensland − Springfield Campus, Springfield Central, QLD 4300, Australia*

Complete contact information is available at: https://pubs.acs.org/10.1021/acsomega.6c03084

Author Contributions

Conceptualization: L.P.; Methodology: T.T.W. and L.P.; Investigation: T.T.W. and P.N.; Project administration: L.P.; Supervision: L.P.; Writing − original draft: T.T.W. and F.U.; Writing − review and editing: L.P., F.U., and J.L.

Notes

The authors declare no competing financial interest.

■ ACKNOWLEDGMENTS

The authors gratefully acknowledge the Second Century Fund (C2F), Chulalongkorn University, for providing financial support through the postdoctoral research fellowship. The authors also express their sincere appreciation to CrystalLyte Co., Ltd., for supplying the graphene quantum dots used in this study.

■ REFERENCES

(1) Reches, Y. Nanoparticles as concrete additives: Review and perspectives. *Construction and Building Materials* **2018**, *175*, 483−495.

(2) Guler, S.; Türkmenoğlu, Z. F.; Ashour, A. Performance of single and hybrid nanoparticles added concrete at ambient and elevated temperatures. *Construction and Building Materials* **2020**, *250*, No. 118847.

(3) Vallurupalli, K.; Meng, W.; Liu, J.; Khayat, K. H. Effect of graphene oxide on rheology, hydration and strength development of cement paste. *Construction and Building Materials* **2020**, *265*, No. 120311.

(4) GivKashi, M. R.; Tohidloo, M. The effect of freeze-thaw cycles and sulfuric acid attack separately on the compressive strength and microstructure of 3D-printed air-entrained concrete. *Construction and Building Materials* **2024**, *440*, No. 137411.

(5) Balakrishnan, B.; Maghfouri, M.; Alimohammadi, V.; Asadi, I.; Roychand, R. The acid and chloride permeability resistance of masonry cement plaster mortar incorporating high-volume fly ash content. *Journal of Building Engineering* **2024**, *86*, No. 108783.

(6) Ghoddousi, P.; Zareechian, M.; Shirzadi Javid, A. A.; Habibnejad Korayem, A. Microstructural study and surface properties of concrete pavements containing nanoparticles. *Construction and Building Materials* **2020**, *262*, No. 120103.

https://doi.org/10.1021/acsomega.6c03084
ACS Omega XXXX, XXX, XXX−XXX

(7) Zhao, L.; Guo, X.; Song, L.; Song, Y.; Dai, G.; Liu, J. An intensive review on the role of graphene oxide in cement-based materials. *Construction and Building Materials* **2020**, *241*, No. 117939.
(8) Win, T. T.; Prasittisopin, L.; Jongvivatsakul, P.; Likitlersuang, S. Investigating the synergistic effect of graphene nanoplatelets and fly ash on the mechanical properties and microstructure of calcium aluminate cement composites. *Journal of Building Engineering* **2023**, *78*, No. 107710.
(9) Jiang, Z.; Sevim, O.; Ozbulut, O. E. Mechanical properties of graphene nanoplatelets-reinforced concrete prepared with different dispersion techniques. *Construction and Building Materials* **2021**, *303*, No. 124472.
(10) Du, H.; Gao, H. J.; Pang, S. D. Improvement in concrete resistance against water and chloride ingress by adding graphene nanoplatelet. *Cem. Concr. Res.* **2016**, *83*, 114−123.
(11) Basquiroto de Souza, F.; Yao, X.; Lin, J.; Naseem, Z.; Tang, Z. Q.; Hu, Y.; Gao, W.; Sagoe-Crentsil, K.; Duan, W. Effective strategies to realize high-performance graphene-reinforced cement composites. *Construction and Building Materials* **2022**, *324*, No. 126636.
(12) Devi, S. C.; Khan, R. A. Effect of graphene oxide on mechanical and durability performance of concrete. *Journal of Building Engineering* **2020**, *27*, No. 101007.
(13) Hulagabali, M. M.; Vesmawala, G. R.; Patil, Y. D. Synthesis, characterization, and application of graphene oxide and reduced graphene oxide and its influence on rheology, microstructure, and mechanical strength of cement paste. *Journal of Building Engineering* **2023**, *71*, No. 106586.
(14) Shamsaei, E.; de Souza, F. B.; Yao, X.; Benhelal, E.; Akbari, A.; Duan, W. Graphene-based nanosheets for stronger and more durable concrete: A review. *Construction and Building Materials* **2018**, *183*, 642−660.
(15) Alateah, A. H. Graphene concrete: Recent advances in production methods, performance properties, environmental impact and economic viability. *Case Studies in Construction Materials* **2023**, *19*, No. e02653.
(16) Tragazikis, I. K.; Dassios, K. G.; Dalla, P. T.; Exarchos, D. A.; Matikas, T. E. Acoustic emission investigation of the effect of graphene on the fracture behavior of cement mortars. *Engineering Fracture Mechanics* **2019**, *210*, 444−451.
(17) Mohammed, A.; Sanjayan, J. G.; Duan, W. H.; Nazari, A. Incorporating graphene oxide in cement composites: A study of transport properties. *Construction and Building Materials* **2015**, *84*, 341−347.
(18) Du, H. J.; Pang, S. D. Transport of water and chloride ion in cement composites modified with graphene nanoplatelet. *Key Eng. Mater.* **2015**, *629*, 162−167.
(19) Jin, M.; Jiang, L.; Lu, M.; Bai, S. Monitoring chloride ion penetration in concrete structure based on the conductivity of graphene/cement composite. *Construction and Building Materials* **2017**, *136*, 394−404.
(20) Lv, S.; Ma, Y.; Qiu, C.; Sun, T.; Liu, J.; Zhou, Q. Effect of graphene oxide nanosheets of microstructure and mechanical properties of cement composites. *Construction and Building Materials* **2013**, *49*, 121−127.
(21) Liu, J.; Li, R.; Yang, B. Carbon dots: a new type of carbon-based nanomaterial with wide applications. *ACS Cent. Sci.* **2020**, *6* (12), 2179−2195.
(22) Shi, J.; Tian, G.; Zhang, Z.; Zou, P.; Li, H.; Wang, Y.; Zhang, J. Effect of graphene quantum dots and curing ways on properties of serpentine mortar. *Mater. Lett.* **2025**, *385*, No. 138134.
(23) Lawongkerd, J.; Yodprasert, K.; Bubpachat, P.; Prasittisopin, L.; Subjalearndee, N. Suprastructure Graphene Quantum Dots Promote Dispersion and Enhance Thermal Transport in Metakaolin-Cement Composites. *ACS Appl. Nano Mater.* **2026**, *9*, 10161.
(24) Win, T. T.; Prasittisopin, L.; Nganglumpoon, R.; Pinthong, P.; Watmanee, S.; Tolek, W.; Panpranot, J. Innovative GQDs and supra-GQDs assemblies for developing high strength and conductive cement composites. *Construction and Building Materials* **2024**, *421*, No. 135693.
(25) Win, T. T.; Prasittisopin, L.; Nganglumpoon, R.; Pinthong, P.; Watmanee, S.; Tolek, W.; Panpranot, J. Chemo-physical mechanisms of high-strength cement composites with suprastructure of graphene quantum dots. *Cleaner Materials* **2024**, *11*, No. 100229.
(26) *ASTM C150−12, Standard Specification for Portland Cement*; American Society of Testing Materials: West Conshohocken, 2012.
(27) *ASTM C33−18, Standard Specification for Concrete Aggregates*; American Society of Testing Materials: West Conshohocken, 2018.
(28) Panpranot, J.; Nganglumpoom, R.; Teerawatananond, T.; Watmanee, S.; Pinthong, P.; Poolboon, K.; Hongrutai, N.; Tungasmita, D.; Tungasmita, S.; Boonyongmaneerat, Y.Electrolytic Process for Producing a Nanocrystalline Carbo n with 1 D, 2d, or 3d Structure And/Or a Nanocrystalline Diamond And/Or a n Amorphous Carbon And/Or a metal-carbon Nanomaterial Composite And/Or a Mixture Thereof at Ambient Conditions. WO2022185098A1, **2022**.
(29) *BS EN 12390−3:2002, Testing hardened concrete, Part 3: Compressive strength of test specimens*; British Standards Institution: Brussels, 2002.
(30) *BS EN 12390−6:2009, Testing hardened concrete, Part 6: Tensile splitting strength of test specimens*; British Standards Institution: Brussels, 2009.
(31) *BS EN 12390−5:2009, Testing hardened concrete, Part 5: Flexural strength of test specimens*; British Standards Institution: Brussels, 2009.
(32) *ASTM C642−21, Standard Test Method for Density, Absorption, and Voids in Hardened Concrete*; American Society of Testing Materials: West Conshohocken, **2021**.
(33) Raj, A.; Yamkasikorn, P.; Kunawisarut, A.; Ngamkhanong, C.; Jongvivatsakul, P.; Prasittisopin, L.; Panpranot, J.; Kaewunruen, S. Enhancing recycled aggregate concrete with graphene quantum dots (GQDs): Refining wastes from construction demolitions and out-of-service railway sleepers. *Developments in the Built Environment* **2025**, *23*, No. 100729.
(34) Flatt, R. J.28 - Conclusions and outlook on the future of concrete admixtures. In *Science and Technology of Concrete Admixtures*, Aïtcin, P.-C., Flatt, R. J., Eds.; Woodhead Publishing, 2016, pp 527−530.
(35) Aïtcin, P.-C.; Flatt, R. J.*Science and technology of concrete admixtures*; Woodhead publishing, 2015.
(36) Raj, A.; Yamkasikorn, P.; Wangtawesap, R.; Win, T. T.; Ngamkhanong, C.; Jongvivatsakul, P.; Prasittisopin, L.; Panpranot, J.; Kaewunruen, S. Effect of Graphene Quantum Dots (GQDs) on the mechanical, dynamic, and durability properties of concrete. *Construction and Building Materials* **2024**, *441*, No. 137597.
(37) Yodprasert, K.; Lawongkerd, J.; Nuntawattananukula, S.; Prasittisopin, L.; Nuaklong, P.; Sanit-in, P. K. Synergistic role of supra-GQDs on the mechanical and durability properties of metakaolin-modified concrete. *Results in Engineering* **2026**, *30*, No. 110290.
(38) Sun, S.; Ding, S.; Han, B.; Dong, S.; Yu, X.; Zhou, D.; Ou, J. Multi-layer graphene-engineered cementitious composites with multi-functionality/intelligence. *Composites Part B: Engineering* **2017**, *129*, 221−232.
(39) Zhao, L.; Guo, X.; Ge, C.; Li, Q.; Guo, L.; Shu, X.; Liu, J. Mechanical behavior and toughening mechanism of polycarboxylate superplasticizer modified graphene oxide reinforced cement composites. *Composites Part B: Engineering* **2017**, *113*, 308−316.
(40) Duan, L.; Zhang, J.; Ma, G.; Pan, Z. Graphene oxide-enhanced nucleation and growth of calcium-silicate-hydrate gel at nanoscale: A molecular dynamics study. *Langmuir* **2024**, *40* (46), 24330−24337.
(41) Qureshi, T. S.; Panesar, D. K. Impact of graphene oxide and highly reduced graphene oxide on cement based composites. *Construction and Building Materials* **2019**, *206*, 71−83.
(42) Mowlaei, R.; Lin, J.; Basquiroto de Souza, F.; Fouladi, A.; Habibnejad Korayem, A.; Shamsaei, E.; Duan, W. The effects of graphene oxide-silica nanohybrids on the workability, hydration, and mechanical properties of Portland cement paste. *Construction and Building Materials* **2021**, *266*, No. 121016.
(43) Li, X.; Liu, Y. M.; Li, W. G.; Li, C. Y.; Sanjayan, J. G.; Duan, W. H.; Li, Z. Effects of graphene oxide agglomerates on workability,

https://doi.org/10.1021/acsomega.6c03084
ACS Omega XXXX, XXX, XXX−XXX

hydration, microstructure and compressive strength of cement paste. *Construction and Building Materials* **2017**, *145*, 402−410.
(44) Win, T. T.; Raengthon, N.; Prasittisopin, L. Advanced Cement Composites: Investigating the Role of Graphene Quantum Dots in Improving Thermal and Mechanical Performance. *Journal of Building Engineering* **2024**, *96*, No. 110556.
(45) Mukherjee, K.; Rajender, A.; Samanta, A. K.A review on the fresh properties, mechanical and durability performance of graphene-based cement composites. *Mater. Today: Proc.***2023**. DOI: .
(46) Hong, X.; Lee, J. C.; Qian, B. Mechanical properties and microstructure of high-strength lightweight concrete incorporating graphene oxide. *Nanomaterials* **2022**, *12* (5), 833.
(47) Mokhtar, M. M.; Abo-El-Enein, S. A.; Hassaan, M. Y.; Morsy, M. S.; Khalil, M. H. Mechanical performance, pore structure and micro-structural characteristics of graphene oxide nano platelets reinforced cement. *Construction and Building Materials* **2017**, *138*, 333−339.
(48) Kashif Ur Rehman, S.; Kumarova, S.; Ali Memon, S.; Javed, M. F.; Jameel, M. A review of microscale, rheological, mechanical, thermo-electrical and piezoresistive properties of graphene based cement composite. *Nanomaterials* **2020**, *10* (10), 2076.
(49) Guo, L.; Wu, J.; Wang, H. Mechanical and perceptual characterization of ultra-high-performance cement-based composites with silane-treated graphene nano-platelets. *Construction and Building Materials* **2020**, *240*, No. 117926.
(50) Long, W.-J.; Wei, J.-J.; Xing, F.; Khayat, K. H. Enhanced dynamic mechanical properties of cement paste modified with graphene oxide nanosheets and its reinforcing mechanism. *Cement and Concrete Composites* **2018**, *93*, 127−139.
(51) Wang, Y.; Pan, C.; Chu, W.; Vipin, A. K.; Sun, L. Environmental remediation applications of carbon nanotubes and graphene oxide: Adsorption and catalysis. *Nanomaterials* **2019**, *9* (3), 439.
(52) Indukuri, C. S. R.; Nerella, R. Enhanced transport properties of graphene oxide based cement composite material. *Journal of Building Engineering* **2021**, *37*, No. 102174.
(53) Pan, Z.; He, L.; Qiu, L.; Korayem, A. H.; Li, G.; Zhu, J. W.; Collins, F.; Li, D.; Duan, W. H.; Wang, M. C. Mechanical properties and microstructure of a graphene oxide−cement composite. *Cement and Concrete Composites* **2015**, *58*, 140−147.
(54) He, R.; Ma, H.; Hafiz, R. B.; Fu, C.; Jin, X.; He, J. Determining porosity and pore network connectivity of cement-based materials by a modified non-contact electrical resistivity measurement: Experiment and theory. *Materials & Design* **2018**, *156*, 82−92.
(55) He, R.; Nantung, T.; Olek, J.; Lu, N. Field study of the dielectric constant of concrete: A parameter less sensitive to environmental variations than electrical resistivity. *Journal of Building Engineering* **2023**, *74*, No. 106938.
(56) He, R.; Ye, H.; Ma, H.; Fu, C.; Jin, X.; Li, Z. Correlating the chloride diffusion coefficient and pore structure of cement-based materials using modified noncontact electrical resistivity measurement. *Journal of Materials in Civil Engineering* **2019**, *31* (3), No. 04019006.
(57) Prasittisopin, L.; Sereewatthanawut, I. Dissolution, nucleation, and crystal growth mechanism of calcium aluminate cement. *Journal of Sustainable Cement-Based Materials* **2019**, *8* (3), 180−197.
(58) Shoukry, H.; Kotkata, M. F.; Abo-El-Enein, S. A.; Morsy, M. S.; Shebl, S. S. Thermo-physical properties of nanostructured lightweight fiber reinforced cementitious composites. *Construction and Building Materials* **2016**, *102*, 167−174.
(59) Prasittisopin, L. Nanotechnology for calcium aluminate cement: thematic analysis. *Reviews on Advanced Materials Science* **2025**, *64* (1), No. 20250180.
(60) Jain, J.; Neithalath, N. Analysis of calcium leaching behavior of plain and modified cement pastes in pure water. *Cement and Concrete Composites* **2009**, *31* (3), 176−185.
(61) Prasittisopin, L.; Nganglumpoon, R.; Thongchom, C.; Panpranot, J. Systematic review and thematic analysis of the utilization of carbon quantum dots (CQDs) in construction materials. *Journal of Materials Science: Materials in Engineering* **2025**, *20* (1), 53.

https://doi.org/10.1021/acsomega.6c03084
ACS Omega XXXX, XXX, XXX−XXX